Technical University of Munich

Chair of Urban Water Systems Engineering

In cooperation with

Environmental Engineering and Earth Sciences, Clemson University

Development of Computational Fluid Dynamics (CFD) Models for Simulating Foulant Reduction by Patterned RO and NF Membranes

Master Thesis

To obtain academic degree

Master of Science (M.Sc.)

Rasna Sharmin

Supervisors:

Dr. David A. Ladner

Environmental Engineering and Earth Sciences, Clemson University

Dr.-Ing. Jörg E. Drewes

Chair of Urban Water Systems Engineering, TUM.

May 2017

Table of Contents

List of Abbreviations

CFD	Computational Fluid Dynamics
UF	Ultra-filtration
MF	Micro-filtration
NF	Nano-filtration
RO	Reverse osmosis
OM	Organic Matter
NOM	Natural Organic Matter
BET	Brunauer–Emmett–Teller
NIL	Nano-Imprinting Lithography
BSA	Bovine serum albumin
PES	Polyethersulfone

List of Figures

Abstract

In this study, CFD simulations were conducted to demonstrate adsorption behavior of membranes with modified surface. Langmuir Adsorption (LA) approach and Modified Langmuir Adsorption (MLA) were used to simulate the adsorption process in membrane system with indirect and direct effect of hydrodynamics respectively. The shear effect has been the key difference between these two approaches. Simulation and comparative analysis for sinusoidal patterned membranes with five different heights are presented here. LA approach was found mostly to depend on the membrane surface area and MLA approach showed the direct effect of change in shear on foulant adsorption for different membrane surface patterns. Membranes with random roughness, trapezoidal and triangular patterns were also simulated using MLA approach and compared to sinusoidal patterned membranes. Membranes with random roughness had more percentages of flux decline than sinusoidal. But trapezoidal and triangular patterns were found to utilize the shear force to have less flux decline and foulant accumulation compared to the sinusoidal pattern.

1 Introduction

Membrane technology is one of the emerging innovations in water treatment and wastewater reuse. Membranes yield treated water with high quality standards and are considered as reliable means of treatment in wastewater treatment facilities (Singh 2006)(Zhang et al. 2013). Membrane processes are typically integrated into a water treatment system like reverse osmosis (RO), nano-filtration (NF), ultra-filtration (UF), micro-filtration (MF) (Šereš et al. 2016). RO and NF are typically suitable for separation of small organics and electrolyte solutes(Bellona et al. 2004)(Verliefde et al. 2017) (Sayed 2010). These processes use hydrostatic pressure gradient and osmotic pressure gradient as driving force (Ho and Sirkar 1992). The main limitation for RO and NF is the permeate flux reduction and pressure drop which are caused by membrane fouling (Vrouwenvelder et al. 2006)(Maruf, Wang, et al. 2013)(Maruf, Rickman, et al. 2013). Different solutes like particles, colloids, salts, organic matters that come from biological wastewater treatment system are highly probable to be adsorbed and accumulated on membrane surface which eventually cause fouling (Xu et al. 2006a). Fouling can be minimized if the system is engineered to prevent or minimize the adhesion of foulants onto membrane surface. The fouling propensity

varies depending on different types of feed water properties (A. Al-Amoudi and Lovitt 2007) (Zhang et al. 2013)(Singh 2006).

Recently several studies are being conducted to find out viable solutions for membrane fouling. One of the proposed solutions is membrane surface modification. In earlier experiments, it has been shown that increased membrane roughness facilitates fouling (Kang and Cao 2012)(Vrijenhoek, Hong, and Elimelech 2001) (Sagle et al. 2009). But later more research showed patterning of membrane surface give better performance against fouling (Lee et al. 2013) (Maruf, Wang, et al. 2013) (Çulfaz et al. 2011). Well defined surface patterns can be very effective in fouling reduction as they control the adhesion and friction of foulants on membrane surface by affecting wetting and mixing of liquid (Feng and Jiang 2006) (Ding et al. 2011) (Stroock et al. 2002) (Stroock et al. 2002) (Ding et al. 2016b). Recently, Membrane Patterning for fouling reduction was investigated by Weinman and Husson(Weinman and Husson 2016). Patterned membrane combined with chemical coating - was the focus of their experiment to get enhanced fouling resistance in crossflow NF system. They found out that a modified membrane had less flux reduction than an unmodified membrane.

The objective of the study is to build a model that can simulate and predict fouling in patterned and non-patterned RO and NF membranes. Both hydrodynamics and solute transport mechanism in the filtration system were modeled and analyzed. For solute transport and adsorption, two scenarios with indirect and direct influence of hydrodynamics were simulated and compared for sinusoidal patterned membrane. The analysis and comparison were mostly done by simulating the models for foulant accumulation and flux decline. Also, possibilities of using other membrane patterns were explored.

2 Background

2.1 Membrane Filtration system

2.1.1 Membrane Fouling

Membrane processes can be called separation process as membrane works as an interphase between two bulk phases (Ho and Sirkar 1992). This fouling mechanism on membrane depends on many factors like membrane characteristics (e.g. material and fabrication, pore size), feed water

characteristics (e.g. solute loading, solute size distribution), hydraulic conditions, operating conditions etc. (Singh 2006)(Zhang et al. 2013). Membrane fouling has four different types: (a) Deposition – from silt and suspended solids, (b) Scaling - form inorganic deposits from soluble salts (c) Biofouling - from microbial growth and (d) organic fouling – from natural or synthetic organics(Kao et al. 2012). Among the membrane foulants, the most important is organic matter (OM) in NF and RO filtration system (A. S. Al-Amoudi 2010). A range of soluble organic compounds present in biologically treated wastewater constitutes the OM. OM can be classified into three classes: (a) Natural Organic Matter (NOM) (b) Synthetic Organic matter (c) Soluble microbial products (Drewes and Fox 1999). NOMs are found to be most active in causing membrane fouling (Xu et al. 2006b). Hydrophobicity of NF Membranes and roughness of RO membranes increases after the adsorption of NOM (Yongki Shim et al. 2002) and protein adsorption (Bowen, Doneva, and Yin 2002) respectively. Due to fouling, Changes in membrane surface characteristics like membrane hydrophobicity, surface charge and surface morphology causes change in membrane performance (Xu et al. 2006b). Pore blocking, concentration polarization and cake formation leads to the reduction of permeate flux and increased flow resistance (Lim and Bai 2003)(Jarusutthirak, Amy, and Croué 2002). Long term fouling can lead to irreversible fouling from microbial action and reduction of membrane lifetime (Lim and Bai 2003).

Concentration polarization in membrane system happens when larger solid particle e.g. macromolecules like proteins are filtered by the membrane. Depending on the type of solid, these form a viscous or gelatinous layer on the membrane surface. This Concentration polarization declines the amount of flux through the membrane (Cheryan and Cheryan 1998). Figure 1 represents the concentration profile with concentration polarization in membrane system. Here the 'gel layer' if formed due to the concentration polarization. Here C_B is the solute concentration in rejected liquid and C_G is the solute concentration in gel layer. Because of this gel layer build up by the solutes near membrane surface a big deviation in solute and flux concentration along membrane occurs.

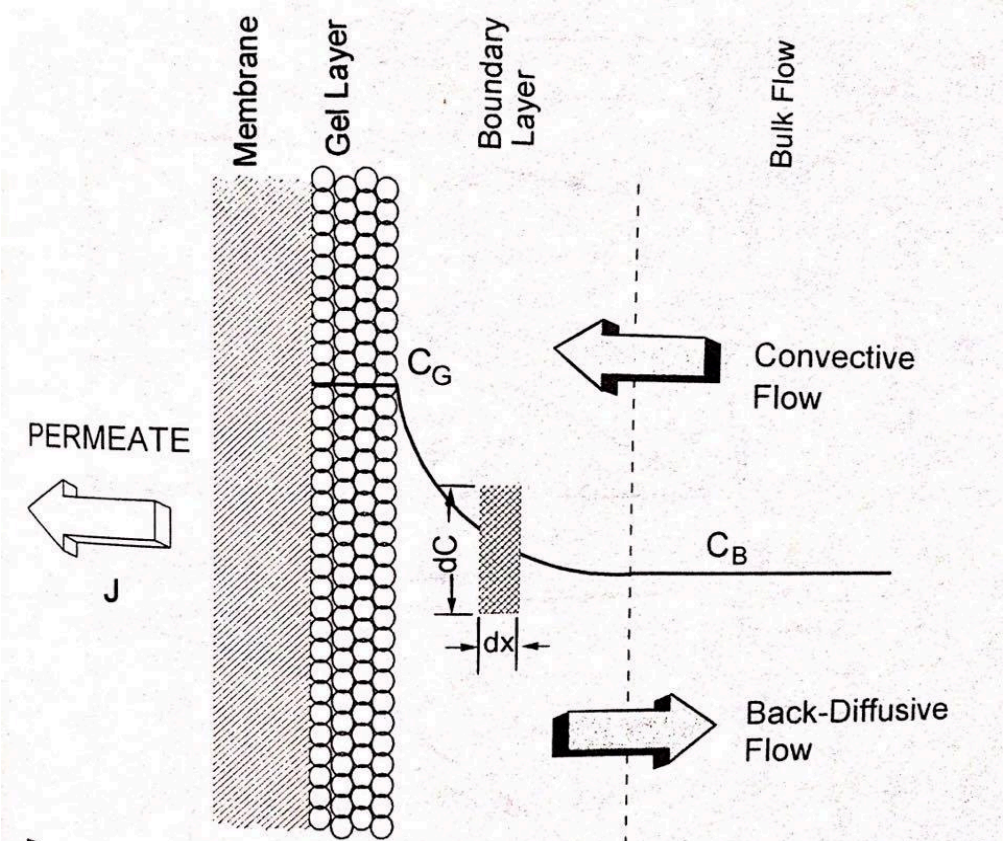

Figure 1 Schematic diagram of concentration polarization on membrane surface showing the buildup gel layer (polarization layer) and boundary layer (Cheryan and Cheryan 1998).

2.1.2 Adsorption Mechanism

In liquid-solid systems, Langmuir, BET and Freundlich isotherms are usually very convenient for environmental modeling, explanation of experimental data and designing equipment (Clark 2009). In CFD modeling of membranes, Langmuir adsorption isotherm concept has been used. Langmuir adsorption isotherm is very well suited for membrane fouling simulation compared to other adsorption isotherms. Figure 2 shows the comparison of Langmuir adsorption with four other adsorption isotherm and it was found to be the best fitted with experimental data after sips (Demneh, Nasernejad, and Modarres 2011).

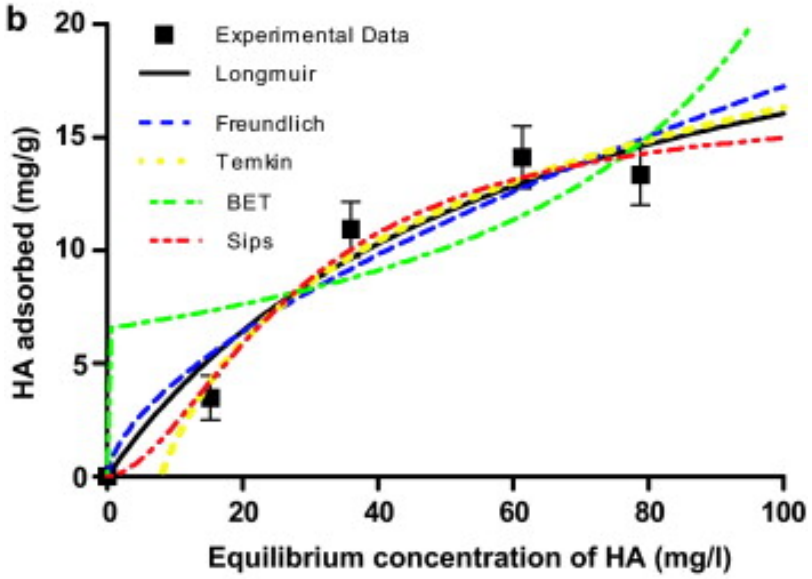

Figure 2: Adsorption isotherms for Humic Acid (HA) adsorption on polyethersulfone membranes (Demneh, Nasernejad, and Modarres 2011)

According to Langmuir isotherm, it is assumed that the rate of desorption is proportional to the amount of solute that occupies the surface (Clark 2009). So,

$$\text{Rate of desorption} = K_2 C_s$$

Here, K_2 is desorption coefficient and C_s is accumulated solute on solid surface.

Hence, the rate of adsorption is proportional to the difference between the concentration of solute at equilibrium and the concentration of accumulated solute on the solid surface. So,

$$\text{Rate of adsorption} = K_1 C (C_{se} - C_s)$$

Here, K_1 is adsorption coefficient, C is concentration of solute in solution and C_{se} is the concentration of accumulated solute on solid surface at equilibrium. So, the change in concentration of accumulated solute on solid surface can be written as following (Clark 2009):

$$\frac{dC_s}{dt} = K_1 C (C_{se} - C_s) - K_2 C_s \qquad (1)$$

In Equation 1, any definite the unit of k_1 and k_2 has not been found so far. (Jones and O'Melia 2000) reported calculation of k_1 and k_2 in his work. Although the units don't agree with equation (1) and don't give the same unit for each term of the equation.

2.2 Membrane Patterning against fouling

Surface patterning is one of the latest trends in the area of physical modification of membrane to reduce fouling. For fouling reduction, two surface modification methods that have been mostly used so far are phase separation micro-molding (Çulfaz et al. 2011)(Laura Vogelaar et al. 2005)(L. Vogelaar et al. 2003)(Gironès et al. 2006)(Bikel et al. 2009) and thermal embossing NIL (Nanoimprint Lithography) process(Wang and Ding 2010)(Chou 1996)(Guo 2007). In phase inversion process, polymer solutions of the membrane are kept in structured molds to solidify and become patterned (Laura Vogelaar et al. 2005). In NIL process, a viscous polymer film is pressed by a nanostructured mold in certain temperature and force (thermal embossing) (Chou 1996)(Weinman and Husson 2016).

The first direct and effective NIL patterning on membrane was reported by (Maruf, Wang, et al. 2013). They used commercial polyethersulfone UF-type membrane and used a silicon mold which had line and spaces with 1:1 ratio. The patterning process was done in 120°C with a pressure of 4MPa for 180s. The patterning process is illustrated in Figure 3a. Figure 3b and Figure 3c shows the change in membrane topographic vertical dimension before and after patterning.

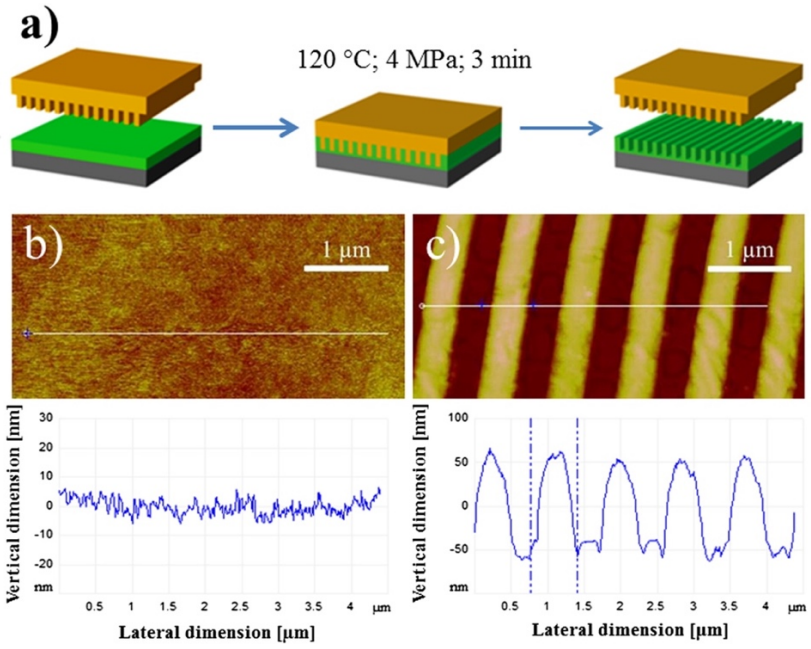

Figure 3: (a) Schematic diagram of NIL process for membrane patterning by line and space silicon mold, topographic AFM image of (b) non-patterned and (c) patterned membrane(Maruf, Wang, et al. 2013)

In this study, they also showed that after patterning the membrane always maintained better flux yield than non-patterned membrane regardless of transmembrane pressure and foulant (silica particle). In a later study (Maruf, Rickman, et al. 2013), they showed that this patterning of UF membranes actually lets the membrane absorb less amount of foulant. In this study, they used Bovine Serum albumin (BSA) as foulant.

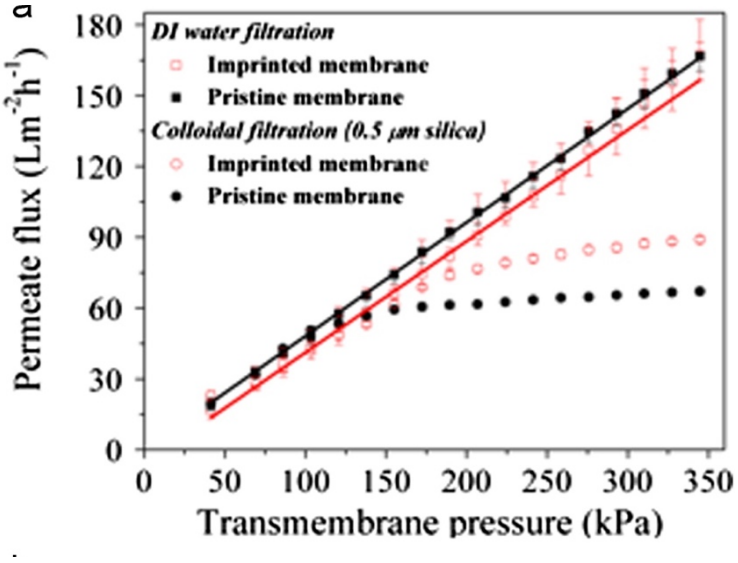

Figure 4: Permeate flux yield in different transmembrane pressure for imprinted (patterned) and pristine (non-patterned) membrane both for DI water (no foulant) and colloidal (with silica foulant) filtration (Maruf, Wang, et al. 2013).

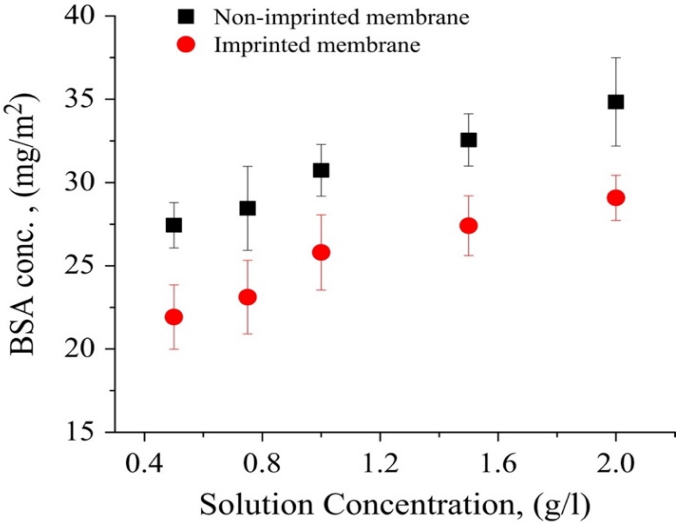

Figure 5: BSA adsorption isotherm for non-imprinted (non-patterned) and imprinted (patterned) PES membrane (Maruf, Rickman, et al. 2013).

NIL process for surface patterning has been considered to be more convenient (Ding et al. 2016a) and cost effective (Ding et al. 2016a)(Ro et al. 2011). Later, Weinman and Husson (Weinman and Husson 2016) described a method for applying both chemical coating and nano-pattern to modify membrane surface. Figure 6 shows the patterning process using nano-scale line and groove silicon stamp heated at 45°C and with 6670N force. Then putting a chemical coating using Poly(ethylene glycol) diglycidyl ether (PEGDE). They found out that, unmodified membranes had flux decline of 22% in 120 mins. But patterned membranes had 0-8% flux decline depending on the modification.

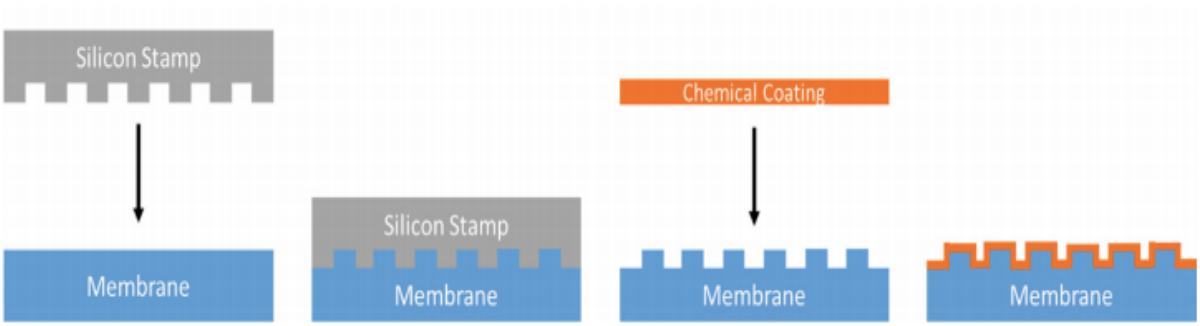

Figure 6 physical patterning on a membrane surface by deformation (Weinman and Husson 2016)

With the flow of feed through the membrane system, particle comes in touch with membrane surface and adheres to it causing fouling. Membrane patterning is showing some promising results to prevent this fouling phenomena. It has been observed that patterning a membrane actually associates to less percentage of surface coverage by foulant and increased permeate flux. (Maruf, Wang, et al. 2013)(Won et al. 2012)(Jang et al. 2015)(Petronis et al. 2000). The probable reasons are hydrodynamic interaction (Jang et al. 2015)(Lee et al. 2013) with membrane surface and increased surface area because of patterning (Gença, Durmaz, and Çulfaz-Emecen 2015).

Patterning a membrane causes change in hydrodynamics in membrane system which helps less attachment of foulant on membrane. Young Ki Lee (Lee et al. 2013) showed in his simulation work that the local shear in patterned membrane is higher than in a flat membrane (Figure 7). He explained that high shear and velocity along the higher regions of the prism pattern and lower shear and velocity in the lower region create a vortex that favors in creating solute aggregation in lower

region. Eventually very low accumulation on upper region of the pattern and high accumulation in lower region is observed. These phenomena were also seen in his experimental work as well.

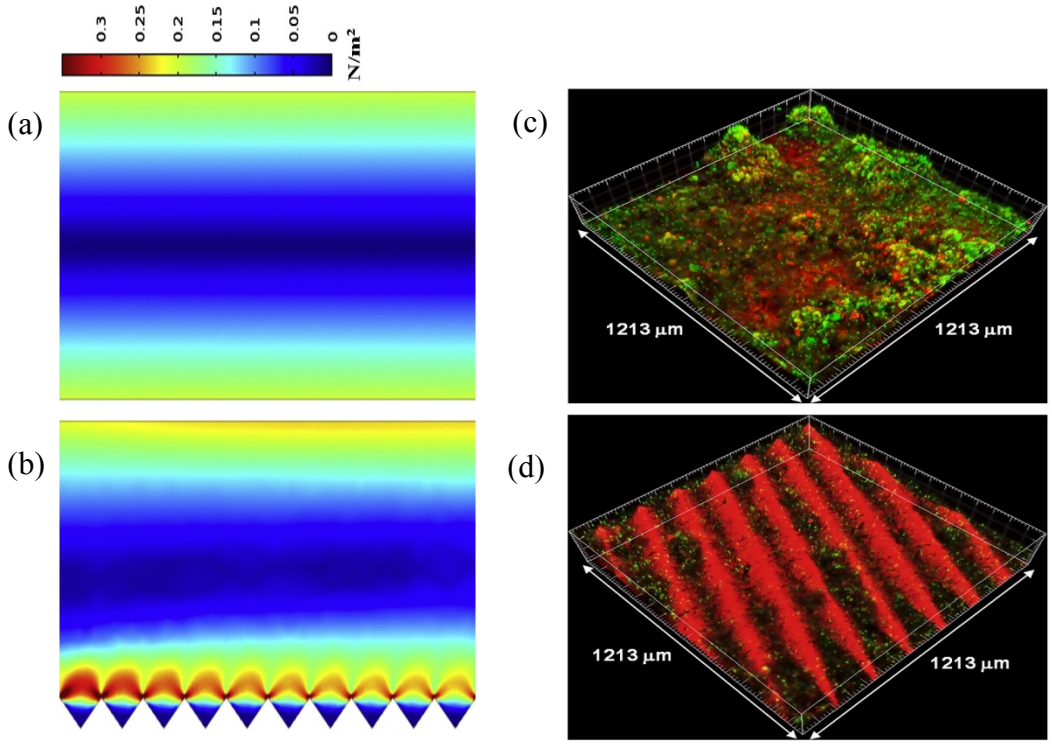

Figure 7: simulated shear stress for (a) flat membrane and (b) prism patterned membrane and confocal microscopy images of microbial (green) on membrane surfaces (red) in experiment: (c) flat membrane and (d) prism patterned membrane. (Lee et al. 2013).

Later, Young-June Won (Won et al. 2016) in his work presented the correlation of fouling with membrane patterning. He compared non-patterned and prism patterned membranes with different heights and found out that total mass attached was highest in non-patterned membrane. He also showed that for larger Reynolds number the higher prism pattern works better but for lower Reynolds number the opposite happens.

In most of the scenario it is seen that patterned membranes yield more flux than non-patterned or flat pressed membrane (Çulfaz et al. 2011)(Vrijenhoek, Hong, and Elimelech 2001)(Weinman and Husson 2016)(Gença, Durmaz, and Çulfaz-Emecen 2015)(Maruf, Wang, et al. 2013)(Lee et al. 2013). One viable reason behind this is the increased surface area because of patterning. In lots of cases, if the flux yield is normalized on membrane surface area, the fouling rate wouldn't be significant (Gença, Durmaz, and Çulfaz-Emecen 2015).

3 Method

For this study, simulation of flow behavior and fouling on membrane surface was done in Comsol Multiphysics 5.2. The geometry properties of sinusoidal membranes and inflow characteristics were taken from Weinman and Husson's work (Weinman and Husson 2016).

3.1 Geometry

In this study, 2D CFD models were constructed to simulate the membrane performance with different pattern geometries.

3.1.1 Sinusoidal

The membrane cross section that was used in the experiment of Weinman and husson (2016) was 1 cm × 2.5 mm. The pattern on the membrane was a sinusoidal pattern with amplitude of 32 nm (64 nm pattern height) and period 625 nm. For modelling, the membrane cross section was downscaled by 1000 keeping the membrane pattern same. Therefore, the developed model was a very small portion of the original membrane cross section in experiment. Figure 8 shows the membrane geometry in model that represents the flat pressed with 0 nm pattern height (Figure 8a) and 'base case' patterned (Figure 8b) membrane with pattern height 64nm in (Weinman and Husson 2016)'s work. Here, pattern height indicates the distance from lowest point of a valley to highest point of a peak of sinusoidal geometry. For better comparison, 3 additional sinusoidal patterned membranes were simulated with same period 625 nm but different pattern height 128 nm, 192 nm and 256 nm (Figure 8(c-e)).

3.1.2 Random roughness

When a membrane is not patterned or pressed, it has random surface roughness. To explore adsorption mechanism of membranes with random roughness and make a comparison with sinusoidal patterned membranes, five different membrane geometries with random surface roughness were constructed and analyzed. Five random geometries are presented in Figure 9 with highest pattern height (height from peak to valley) of 10nm, 64 nm, 128 nm, 192 nm and 256 nm comparable to sinusoidal membranes with pattern height of 0nm, 64 nm, 128 nm, 192 nm and 256 nm respectively.

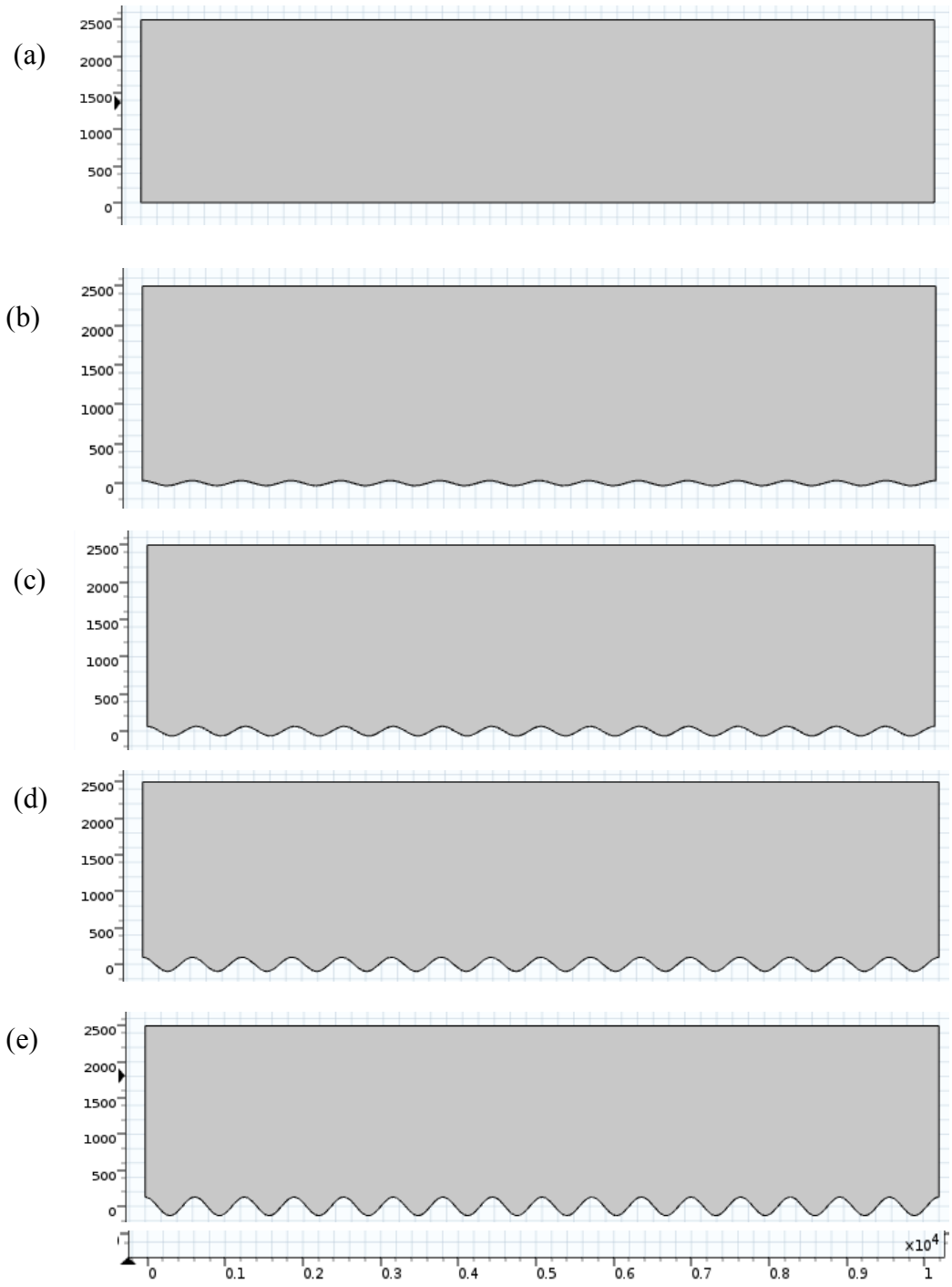

Figure 8 Membranes with different surface patterns with height (a) 0 nm (flat pressed), (b) 64nm (base case), (c) 128 nm, (d) 192 nm and (e) 256 nm

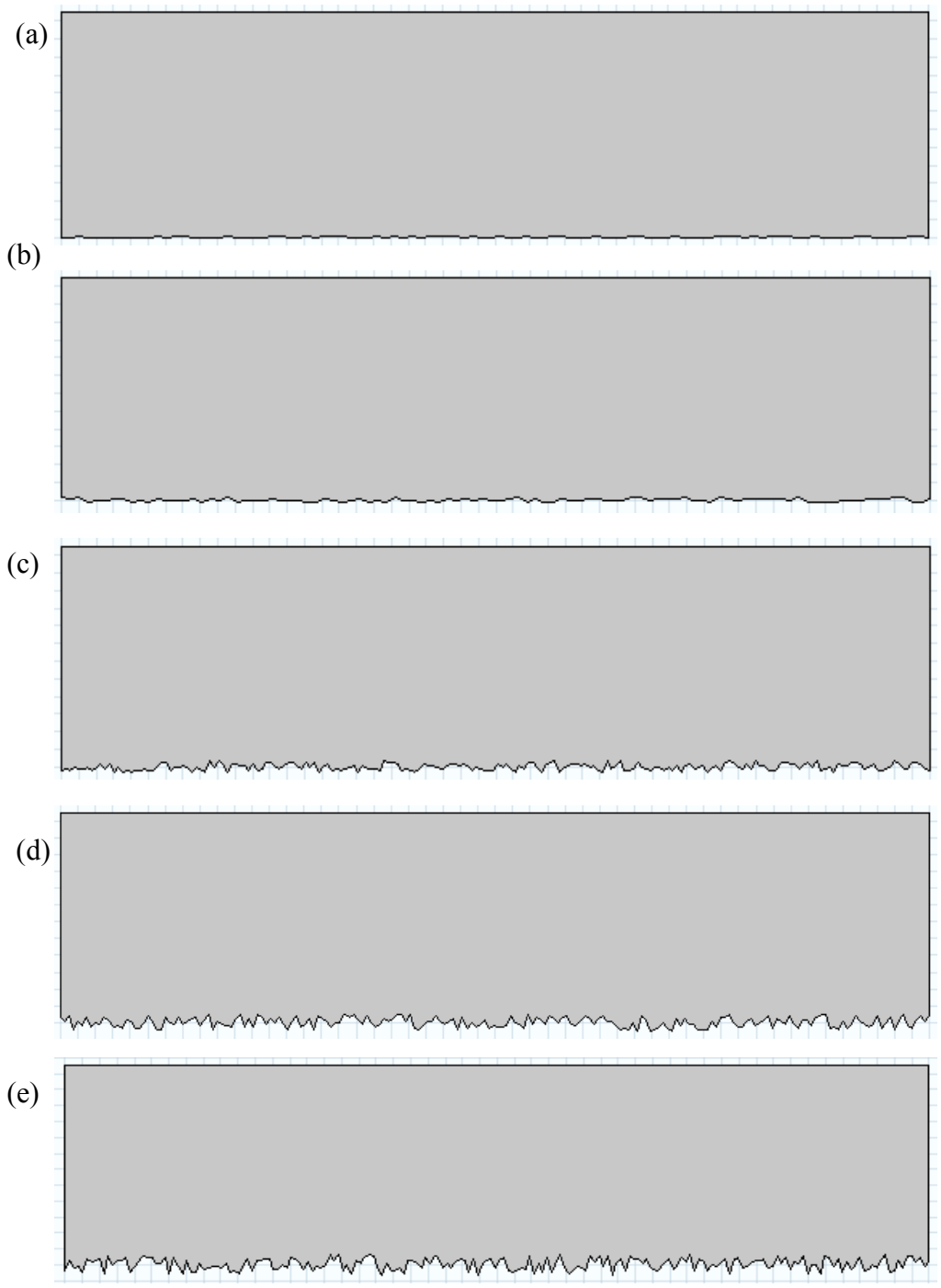

Figure 9 Membrane geometries with random roughness comparable to sinusoidal membranes with pattern highest height (a) 10 nm, (b) 64 nm, (c) 128 nm, (d) 192 nm and (e) 256 nm

3.1.3 Other geometries

Among Other membrane geometries, trapezoidal patterns are viable options. Figure 10a shows trapezoidal geometry with five parameters. By altering one or more than one of the five parameters,

different kinds of geometrical patterns can be achieved. Figure 10(b-d) shows a sinusoidal (base case), a trapezoidal and a triangular membrane geometry. In trapezoidal geometry, b_1 is 625 nm and b_2 is 312.5 nm and in triangular geometry, b_1 is 625 nm and b_2 is 0. These values were chosen to give trapezoidal and triangular patterns same width or period but half of height of sinusoidal pattern to produce shallower valleys. So, in both geometries (Figure 10.b-c), h is 32 nm which makes the valleys shallower than base case membrane (64 nm) (Figure 10a).

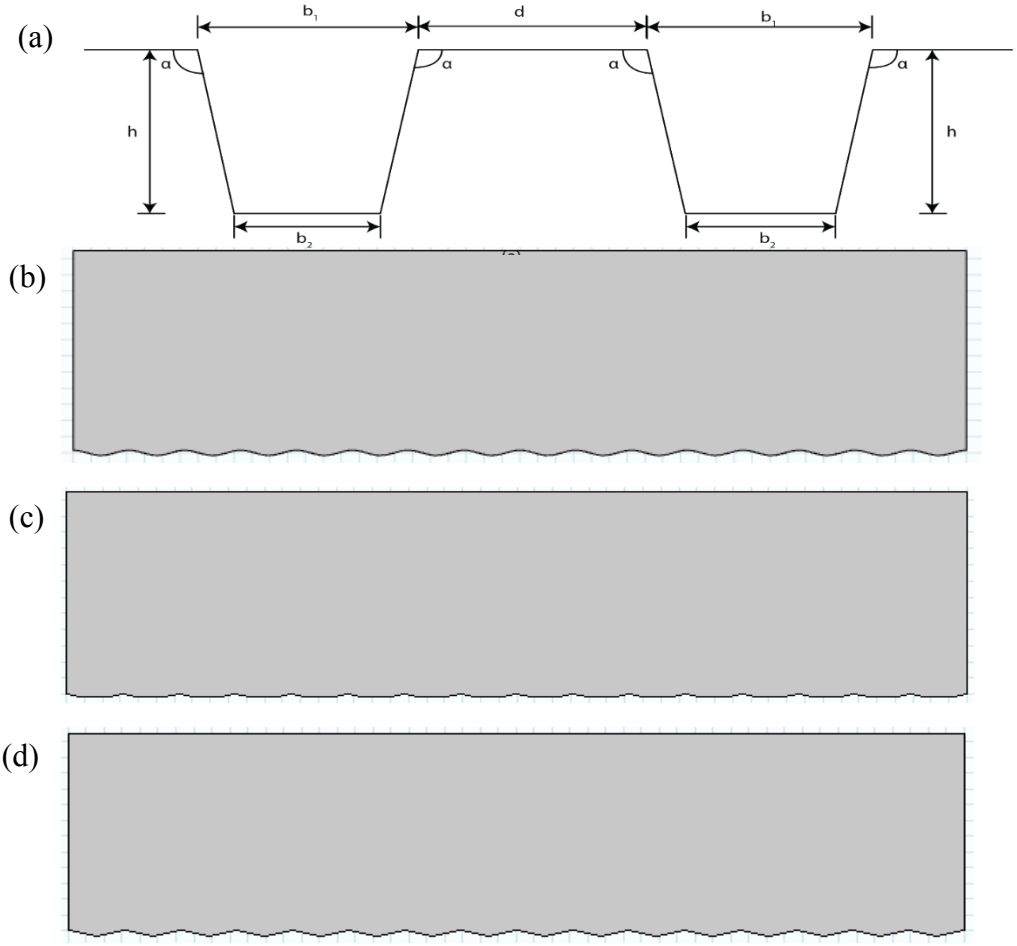

Figure 10: Membrane geometries with (a) sinusoidal base case pattern (b) trapezoidal pattern and (c) triangular pattern

3.2 Model components and boundary condition

3.2.1 Hydrodynamics

For simulation, three computation components that were used are Laminar flow, solute transport and surface reaction. For Laminar flow the boundary conditions are crossflow velocity, pressure

and flux through the membrane. Like the membrane geometry, the crossflow velocity (v_in) was also downscaled from the velocity in experiment 1 m/s to 0.006 m/s using Eq (2). In Eq (2), μ is dynamic viscosity, *dp/dx* is pressure gradient, a is the new membrane height and y is the original membrane height. The values for a and *y* is 2500 nm and 2500 X 10^3 nm respectively. The applied pressure (P) in model was 124 psi which is same as the experiment of Weinman and Husson (Weinman and Husson 2016). The flux (J) though the membrane was defined by Eq (3)

$$U_x = -\frac{1}{2\mu}\frac{dP}{dx}(a^2 - y^2) \tag{2}$$

$$J = \frac{p - \Delta\pi}{\mu R_m}$$

$$= A_m(p - \Delta\pi)$$

$$= A_m(p - a_{osm}C) \tag{3}$$

$$A_m = \frac{J_{initial}}{P} \tag{4}$$

Here, A_m is membrane permeability coefficient, p is pressure, a_{osm} is atmospheric pressure coefficient and C is concentration of foulant in bulk solution.

The value of A_m was calculated by equation (4) where $J_{initial}$ is 120 L/m^2/hr and P is 120 psi. The value of a_{osm} was 4872 Pa/(mol/m^3) and taken from (Xie, Murdoch, and Ladner 2016).

Figure 11 shows assignment of hydrodynamic boundary conditions.

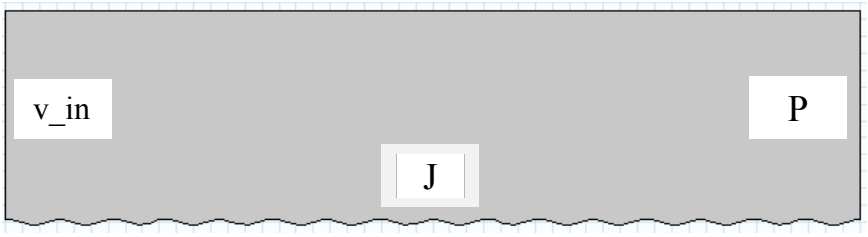

Figure 11: Defining Boundary conditions for hydrodynamics

3.2.2 Foulant transport an adsorption

For solute transport, the inflow concentration of foulant was 0.0721 mol/m^3 which was derived from the concentration of sodium alginate of 30 mg/L reported by Weinman and Husson (Weinman and Husson 2016). It is considered in the model that the amount of foulant that gets adsorbed on the membrane surface is the amount of foulant that is removed from the feed solution near membrane surface and is defined by R. Figure 12 illustrates the boundary condition that are defined for solute transport and surface reaction.

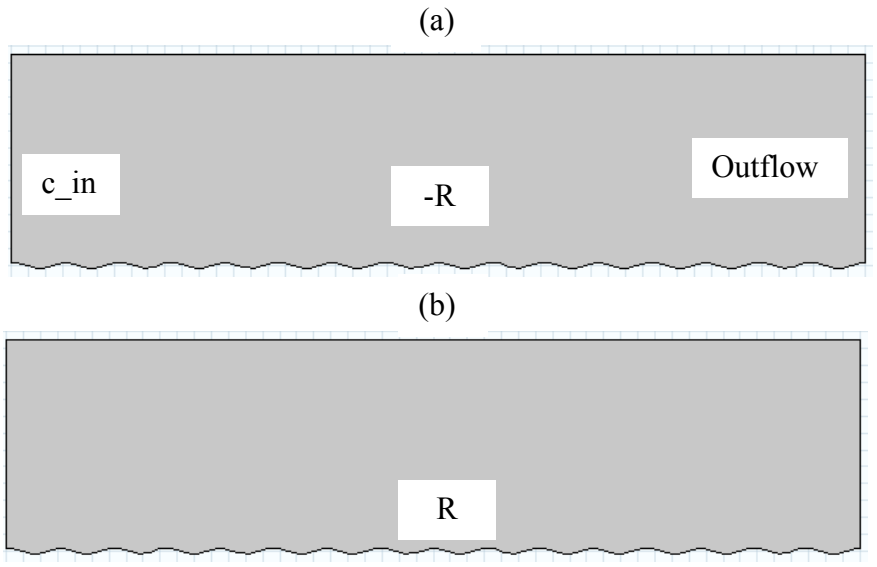

Figure 12: Defining Boundary conditions for foulant transport and adsorption

Here, R represents the change in amount of foulant concentration on membrane surface with time.

To solve R, two kinds of approaches were used for sinusoidal patterned membranes. First approach was using Langmuir adsorption equation (Eq (1). This approach does not take any direct effect of hydrodynamics in consideration. The values used for k_1 was 10^{-3} m^3/mol/s and k_2 was 10^{-6} s^{-1}. In this study the units used for k_1 and k_2 are derived in a way that it gives each term of the adsorption equation same unit.

Second approach was using modified Langmuir equation (Eq (5) which was suggested by (Xie, Murdoch, and Ladner 2016) to include direct hydrodynamic influence on foulant accumulation and flux decline. Desorption of foulant on membrane surface is multiplied by shear stress τ.

$$\frac{dC_s}{dt} = K_1 C(C_{se} - C_s) - K_2 C_s \tau \quad (5)$$

Here, foulant concentration in equlibrium, C_{se} was 1 mol/m^2 for both approaches. The values and units for k_1 and k_2 were changed. The value of k1 was 10^{-1} m^3/mol/s and k2 was 10^{-6} s^{-2}.

3.3 Meshing

The purpose of meshing is to subdivide geometry into 'elements' for modelling and used to solve and represent the solution field of the problems (Frei 2013). For 2D modelling, triangular and quadrilateral (Figure 13) elements and for 3D modelling, tetrahedra, hexahedra, triangular prismatics and pyramid elements are available (Frei 2013). In Figure 13 the black circles are the corners, or 'nodes'. For this study, Physics controlled meshing was done using triangular elements for 2D models which is inbuilt meshing in COMSOL. For membranes with different geometries constitutes different number of domain elements. The meshing for 5 geometries are presented in Figure 14. As, the same type of physics controlled meshing was used for all membranes.

In the zoomed in version of meshing, for flat pressed membrane (Figure 15a) the meshing is uniform all over membrane geometry. But for patterned membrane (Figure 15b) the mesh element size and number varied depending on the change in membrane pattern. When the patterned geometry changes, the models require more mesh elements to make accurate calculations.

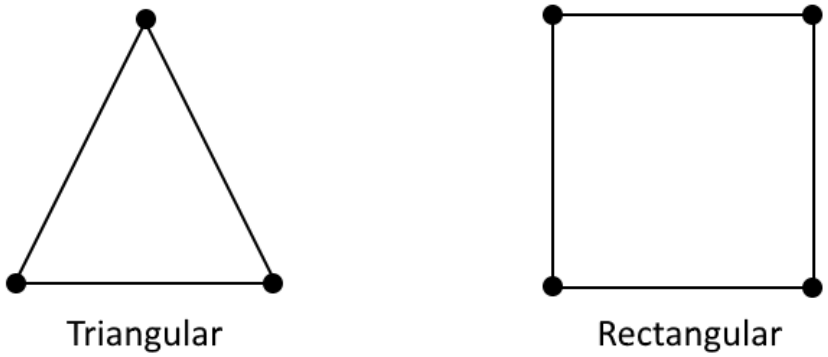

Figure 13 2D modelling elements (Comsol 2016)

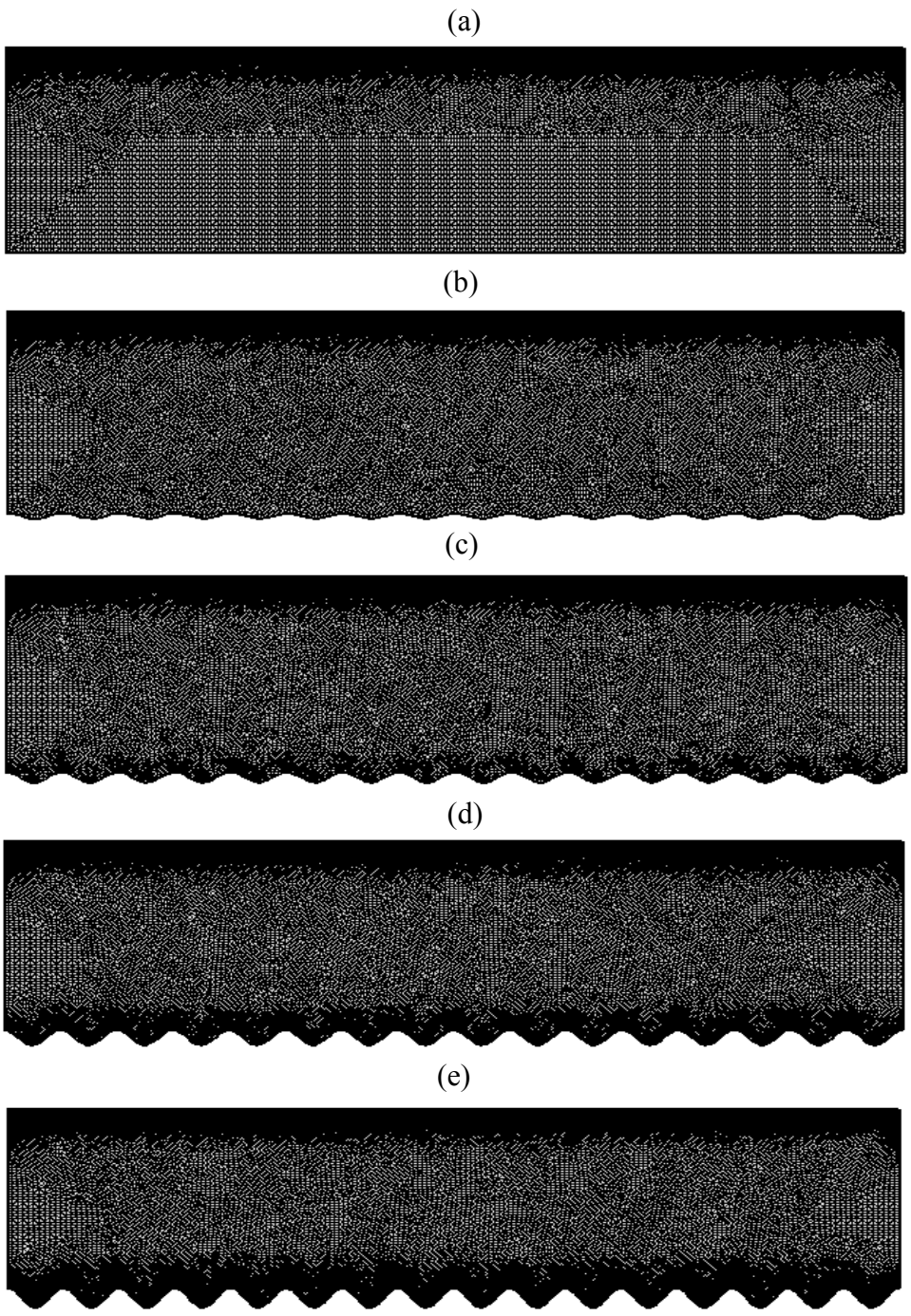

Figure 14: Meshing of sinusoidal membranes with different pattern height (a) 0 nm (b) 64 nm, (c) 128 nm, (d) 192 nm and (e) 256 nm

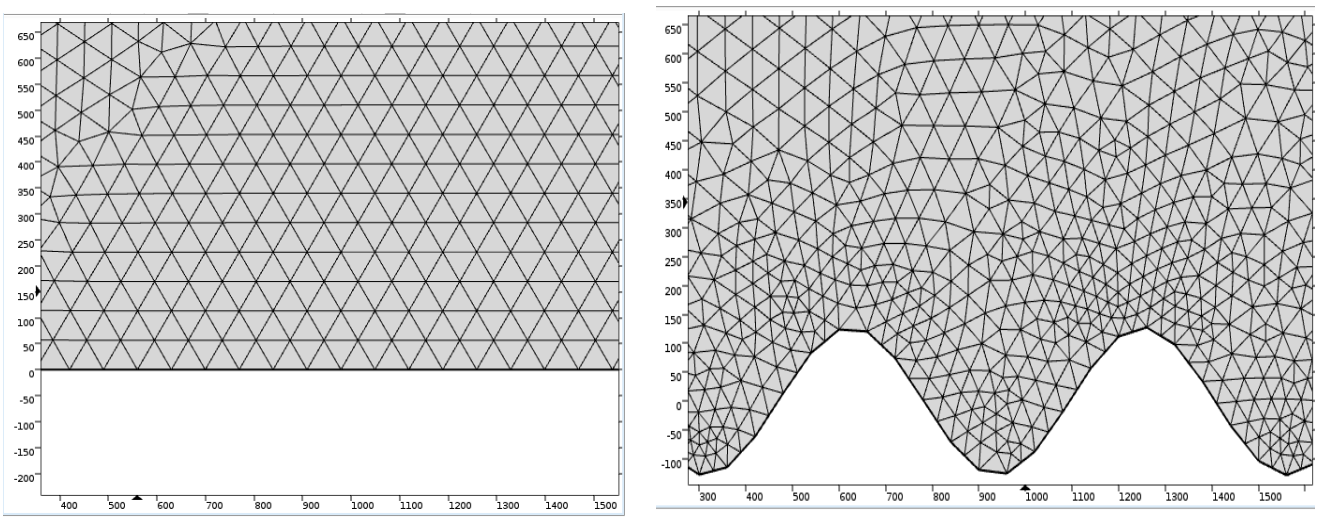

(a) (b)

Figure 15: Zoomed in view of Meshing of sinusoidal membranes with pattern height (a) 0 nm and (b)

3.4 Computation steps

Two step calculation was done for the simulation. In first step, laminar flow modeling was done in steady state condition. In this step, velocity, pressure and shear was calculated. Next, in time dependent step, the solute transport and surface reaction modeling was done using the results from steady state step. Time dependent step calculates change in foulant concentration in bulk solution and on membrane surface. Time dependent calculation was done for 24 hrs for both simulation approach.

4 Results and Discussion

4.1 Hydrodynamic characterization of sinusoidal patterns

4.1.1 Velocity and Pressure Profile

The laminar flow velocity profiles that are generated in steady state step are presented in Figure 16. The white lines represent streamlines through the membrane cross section and red arrows show the fluid flux entrance and exit direction. In all five membranes, the velocity was highest in the center. The zoomed in view of the velocity profiles in Figure 16(a-e) illustrates that stream flows are different among different membrane patterns. The flat pressed membrane had straight stream lines near membrane surface, where 64nm pattern makes the streamlines curved along the membrane surface. In the 256 nm pattern (Figure 16.e), the curved streamlines are more prominent. These different streamline deviations show how the hydrodynamics can be different in different membrane patterns and can have different effects on foulant accumulation. In higher pattern height, the curvature of streamlines are higher which produce more shear stress on the peaks of the patterns. Also, if the pattern height is big enough, the water flow tends to create full vortex which in some extent facilitates foulant aggregation. In Figure 16(e), the curved streamlines in the valleys show initiation of a vortex.

The pressure profiles in Figure 17 represent the pressure change in the membrane as the feed water flows from left to right and through the membrane surface maintaining a fixed flux in steady state. When a membrane is patterned, a difference in pressure can be seen between left and right side of the pattern peak. With increase in pattern height the difference becomes higher. This also gives an indication of change in effect of hydrodynamics with change in membrane pattern.

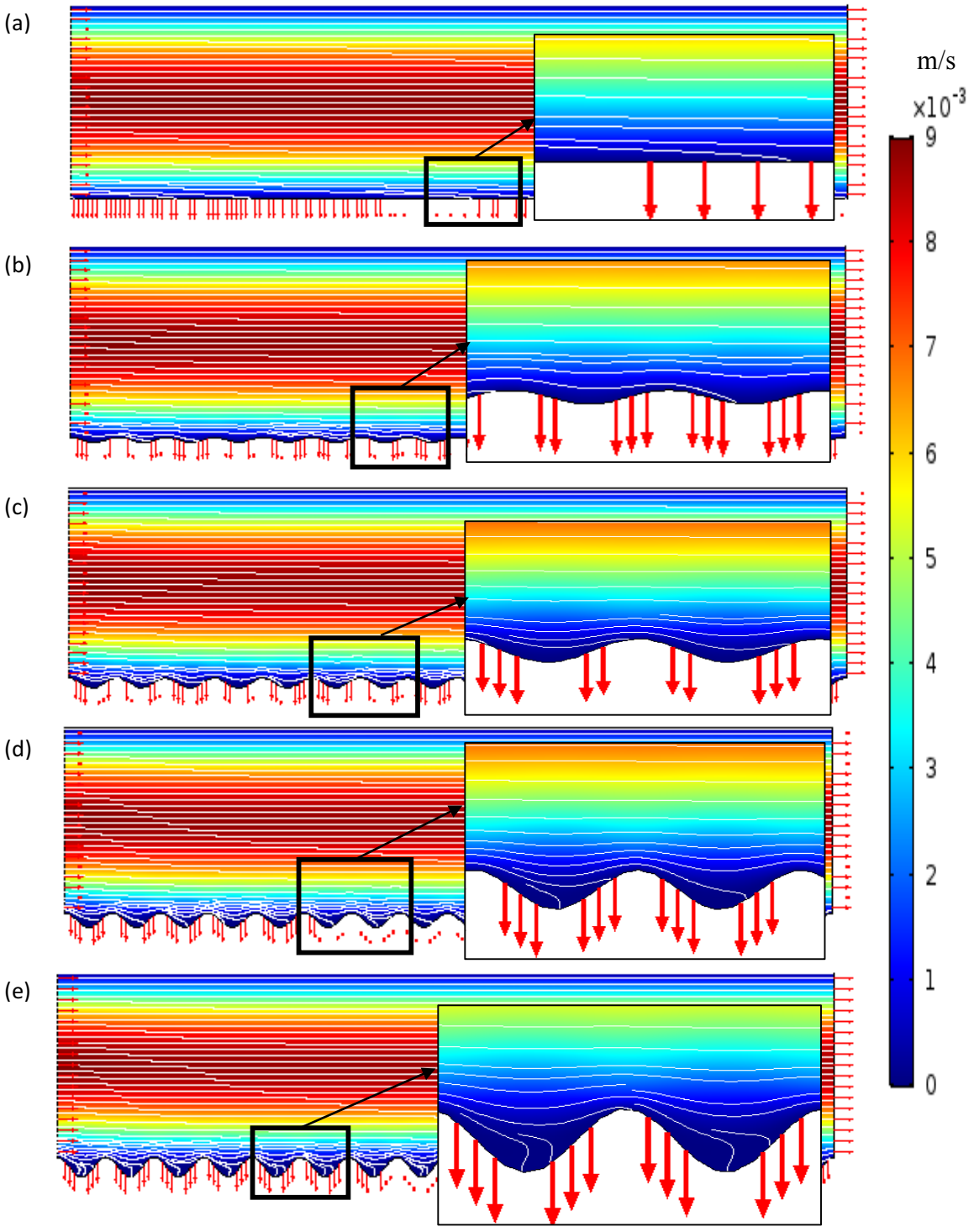

Figure 16: Velocity magnitude profile of sinusoidal membranes with different pattern height (a) 0 nm (b) 64 nm, (c) 128 nm, (d) 192 nm and (e) 256 nm

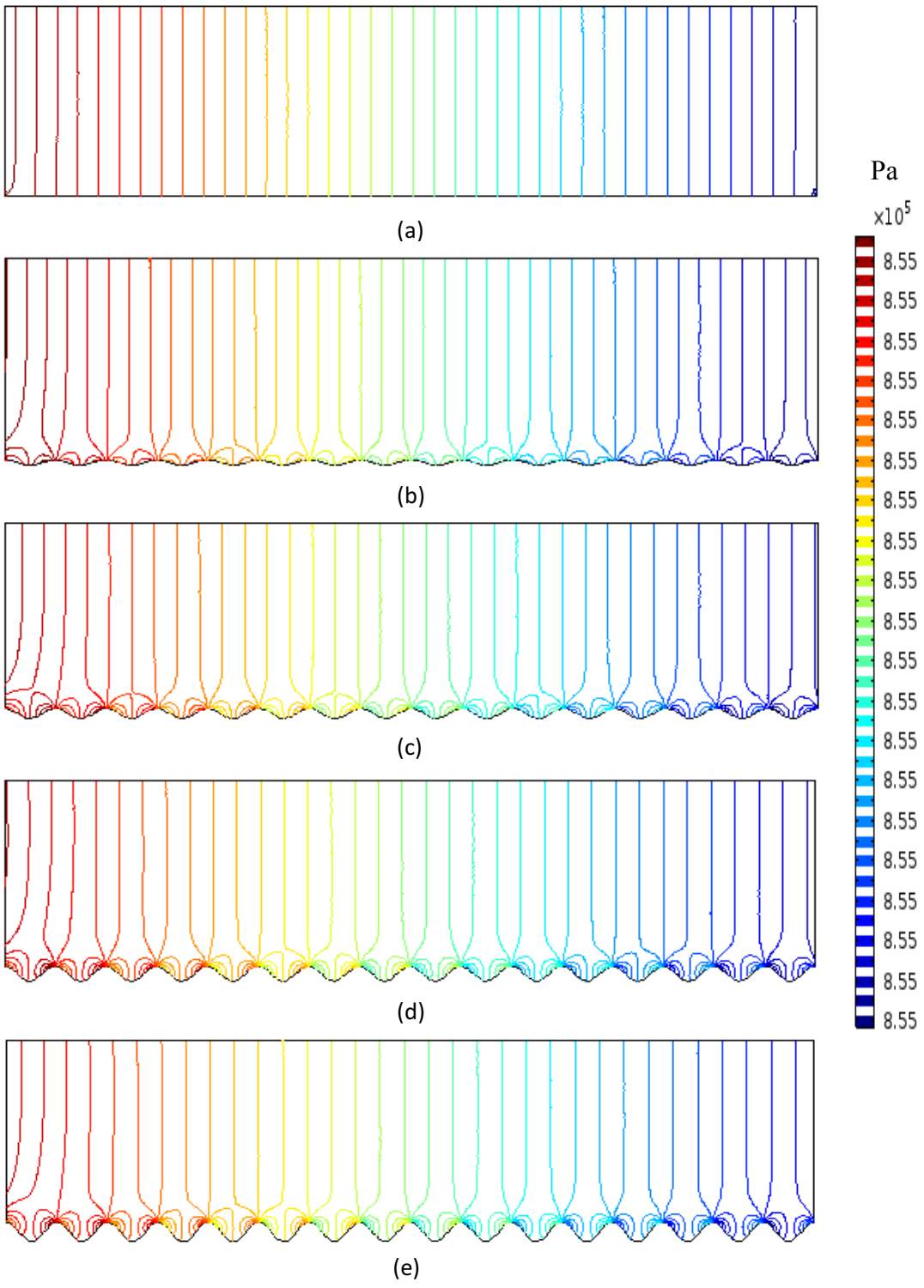

Figure 17: Pressure profile of sinusoidal membranes with different pattern height (a)0 nm (b) 64 nm, (c) 128 nm, (d) 192 nm and (e) 256 nm

4.1.2 Shear profile

As stated in section 4.1.1, the change in streamline direction that happens due to change in surface patterns also causes the change in shear stress along the membrane surface. It can be seen in shear rate along the membrane surface in Figure 18 and shear rate profiles of membrnes in Figure 19. With increase in height of the pattern, the shear stress along peak of the sinusoidal pattern becomes higher. Also, the shear along the pattern valleys becomes smaller with higher pattern height. This is more visible in Figure 18. It illustrates the change in shear rate over the membrane surface at a definite time point (120mins). The flat membrane shows same shear all over the membrane surface and with change in pattern the shear starts to change as well. As seen in Figure 19, the higher shear in peaks than valleys can be seen evidently in Figure 18 as well. Also, the shear in valleys of 256 nm patterned membrane has shear profile with flat end instead of a curve. The reason for this is the shear in that area became zero. It is expected that higher shear will assist in mitigation of foulant adsorbance on membrane surface.

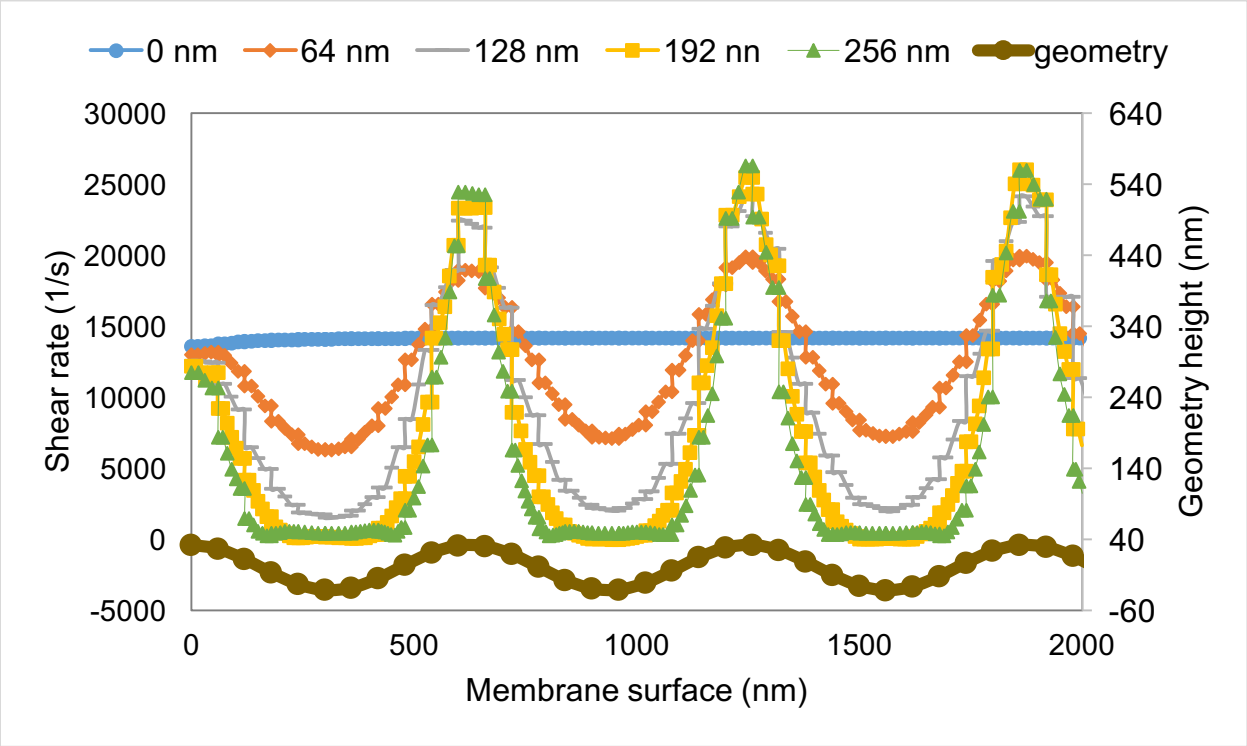

Figure 18: Shear rate along the sinusoidal membrane surface with different pattern height

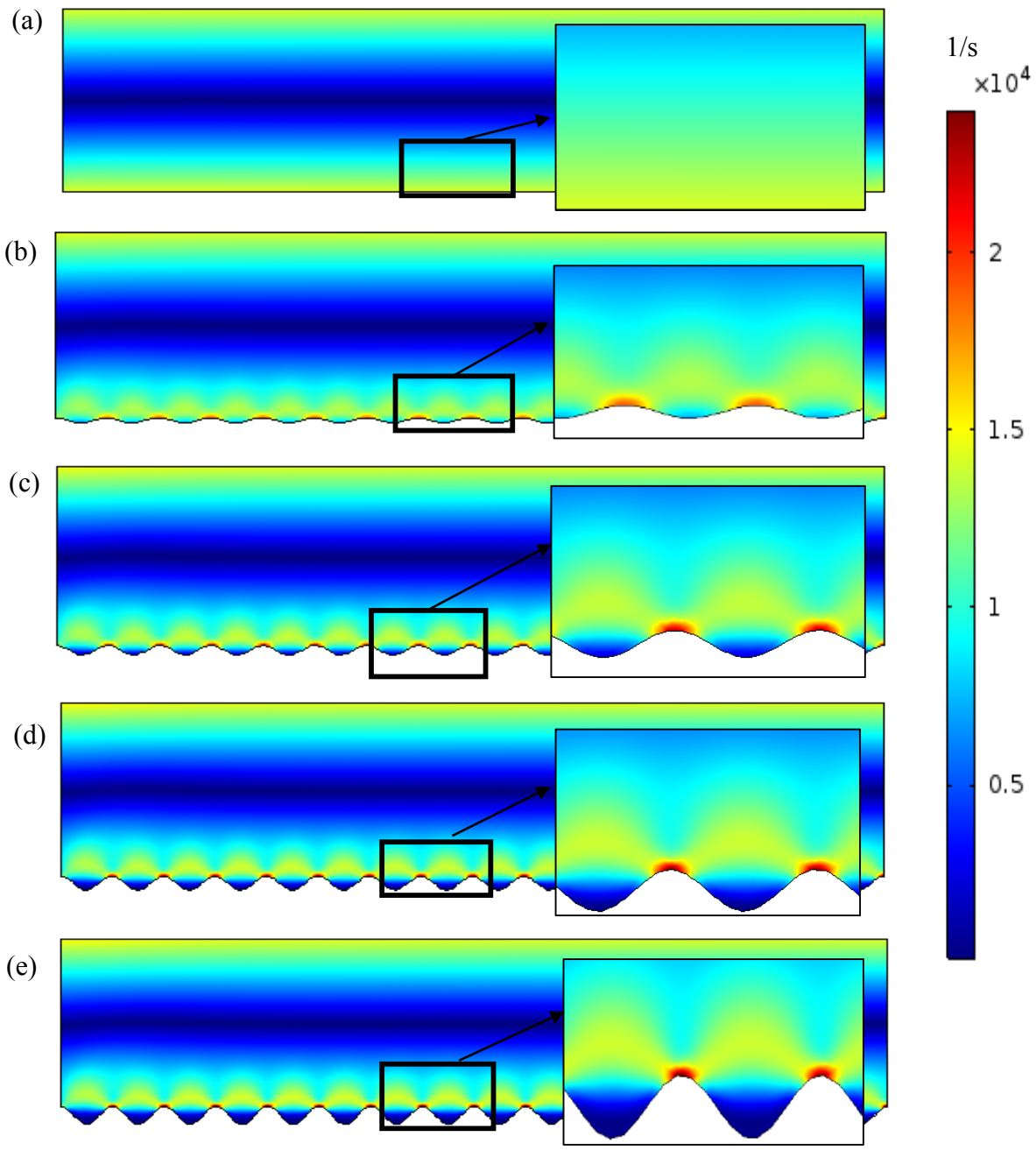

Figure 19: Shear rate profile of sinusoidal membranes with different pattern height (a) 0 nm, (b) 64 nm, (c) 128 nm, (d) 192 nm and (e) 256 nm

4.2 Foulant transport and adsorption for sinusoidal patterns

4.2.1 Langmuir Adsorption (LA) approach

While water passing through, foulant accumulates due to the adsorption on membrane surface. To calculate foulant transport and adsorption, the first approach was using Langmuir adsorption equation (1).

4.2.1.1 Foulant accumulation on membrane surface

In the model, adsorption and desorption in membrane filtration process happens simultaneously until it reaches the equilibrium surface concentration (C_{se}) with time. The adsorption (k_1) and desorption (k_2) coefficients play an important role to control the time that the system takes to reach the equilibrium. Primarily to understand the behavior of the model and accumulation trend, different values of k_1 & k_2 were tried out (described in section 4.2.1.4). Final values used for k_1 & k_2 are 10^{-3} m^3/mol/s and 10^{-6} s^{-1} respectively. Figure 20 shows the average foulant accumulation on membrane surface till it reaches the equilibrium concentration. It took 24 hrs for all five sinusoidal membranes to reach the equilibrium concentration. Here, 24 hrs time refer to the time variable used in the model. The required simulation time for each model was several minutes. Membranes with different pattern height acted differently and took different amount of time to reach equilibrium. The flat membrane with zero pattern height accumulated foulant faster than any other sinusoidal membrane and reached the equilibrium first and 256 nm reached last. Higher the height of the membrane geometry lower the accumulation rate is. Figure 21 shows accumulated foulant on five sinusoidal membranes on a definite time point (120min). The red arrow in Figure 20 showing the time point of 120min (2hr). Figure 21 shows the trend of foulant adsorption on membrane. The foulant keeps accumulating on the membrane surface until it reaches the equilibrium. It can be seen that the amount of adsorbed foulant in more in peaks than the valleys. As Langmuir equation does not have any hydrodynamics effect in it, the model assumes that foulant gets adsorbed the first thing it gets on its way. Eventually the amount of surface concentration (C_s) increases and becomes equal to the equilibrium surface concentration (C_{se}). Then adsorption becomes zero and no additional foulant is adsorbed.

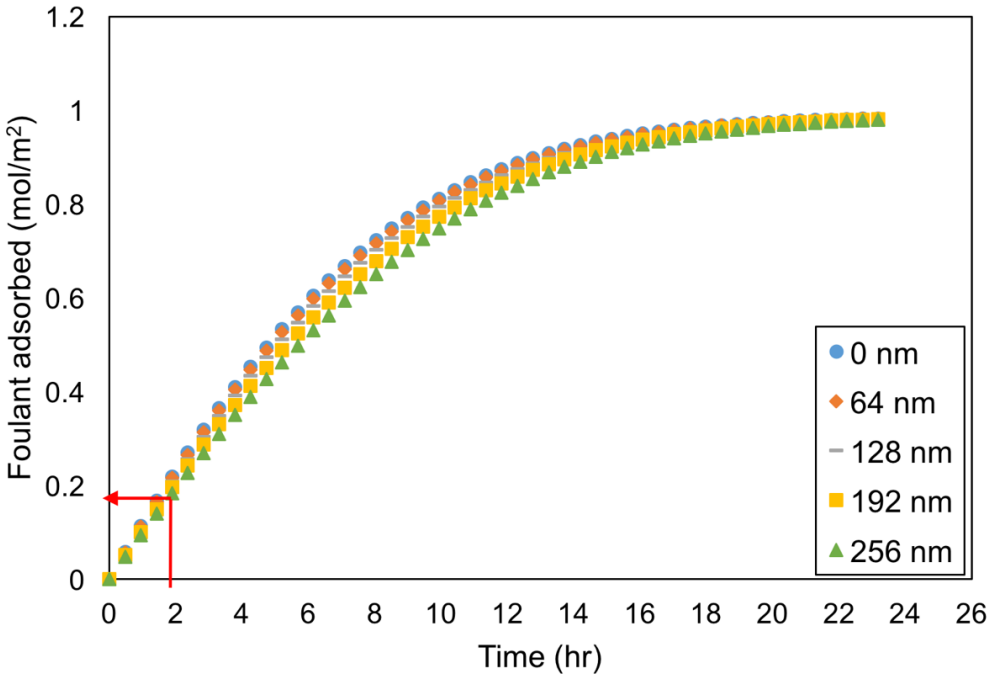

Figure 20: Average foulant accumulation on membrane surface with time for five different sinusoidal membranes.

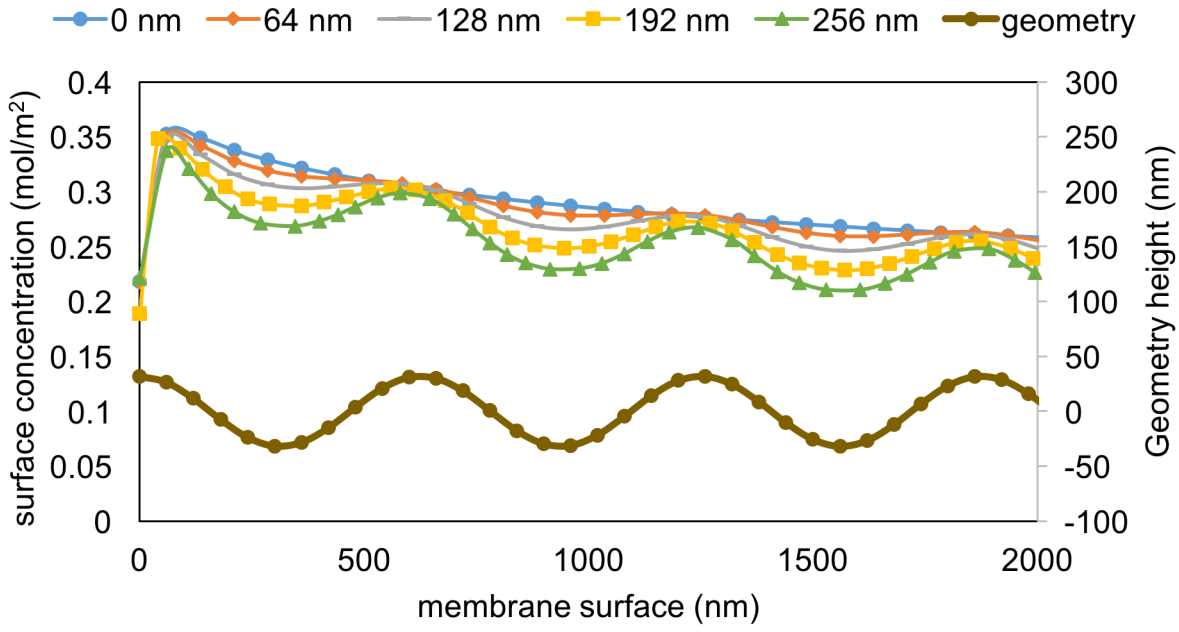

Figure 21 Foulant accumulation on membrane surface for five different sinusoidal membranes on a definite time point (120mins).

4.2.1.2 Bulk concentration

In the model, it is assumed that the amount of foulant that gets adsorbed and accumulates on membrane surface is the amount of foulant that gets removed form feed solution in membrane system. Figure 22 shows the gradual change in bulk concentration (C) in sinusoidal membrane system with pattern height 0nm, 64nm and 256 nm. It has been seen in section 4.2.1.1 that membrane with the smallest pattern height adsorbs foulant and reaches the equilibrium first. The bulk concentration profiles (Figure 22) show the similar situation. 0 nm pattern height reaches the equilibrium faster than 64nm and 256nm. Especially if 0 nm is compared to 256nm in 14hr, it can be seen that 0 nm is about to reach the equilibrium but 256 nm is still adsorbing.

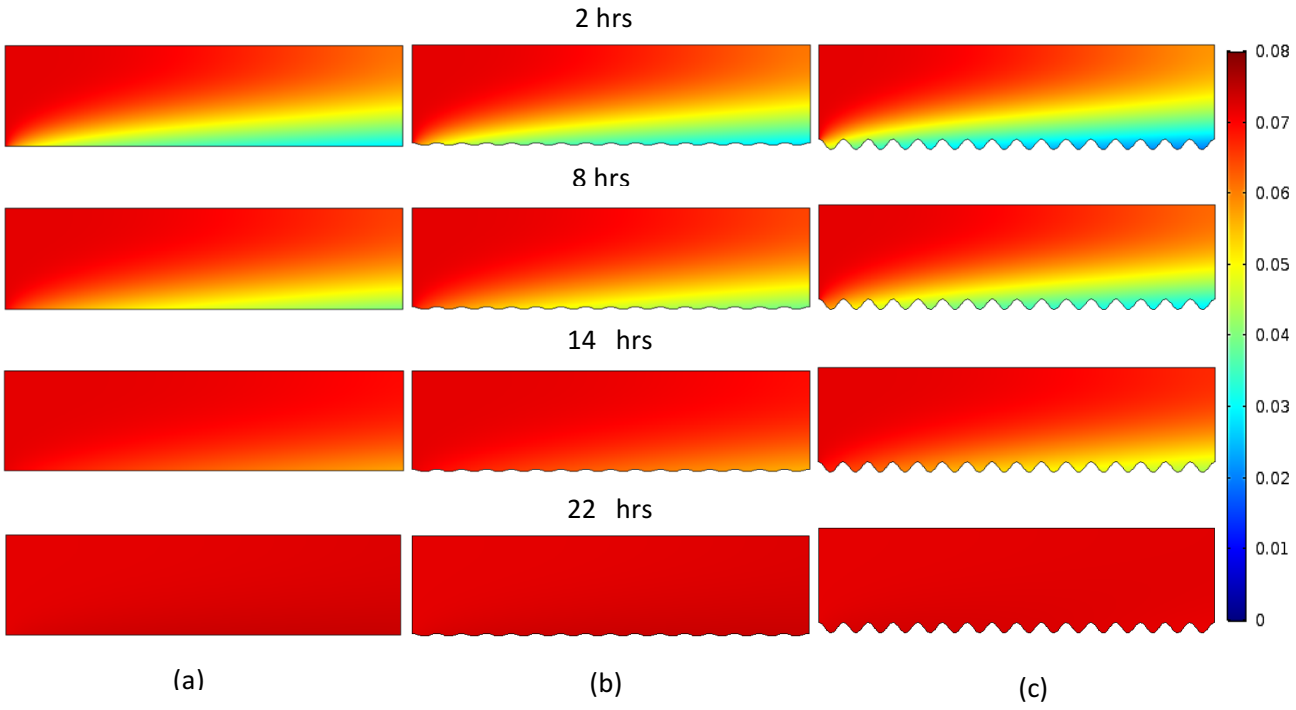

Figure 22: Bulk concentration profiles at different time points of sinusoidal membranes with height (a) 0 nm, (b) 64 nm and (c) 256 nm

4.2.1.3 Flux decline

The flux declines with time due to foulant accumulation on membrane surface. Equation (6) was used to calculate flux. This equation was derived from equation (3) by adding the foulant resistance to the membrane resistance.

$$Flux,\ J = \frac{p - \Delta\pi}{\mu R_m + \mu R_f} \tag{6}$$

$$R_f = C_s F \tag{7}$$

Here, R_f is foulant resistance and F is foulant coefficient.

F is the part of the equation that influence the effect of foulant accumulation on membrane surface on flux decline. Several values for F were tried out to get the desired flux decline pattern that agrees with Weinman and Husson's experimental results (described in section 4.2.1.5) (Weinman and Husson 2016). The value for F that was used here is 2.5×10^{13} m/mol.

Figure 23 shows average flux decline in five membrane geometries over 24 hrs. There is no noticeable change in flux after 17 hrs. This indicates that after 17 hrs the increase in foulant accumulation is too small to make a big change on flux decline. The change in foulant accumulation (Figure 20) and flux decline (Figure 23) seems to be very high in first 10 hrs. In 2 hrs, the flux reaches to 98 L/m^2/hr (for 0 nm). Here, higher pattern height sinusoidal membrane always maintained higher flux. But the difference in % flux decline is very small for different sinusoidal membranes patterns.

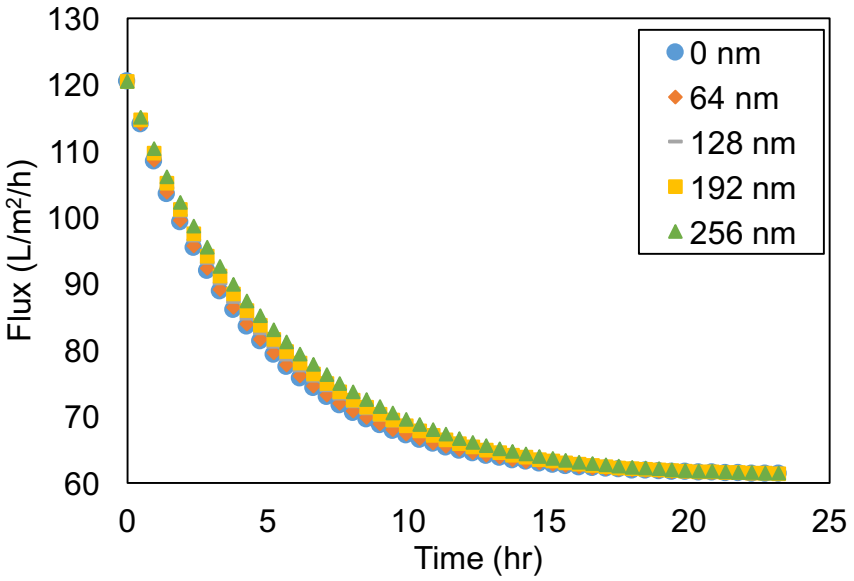

Figure 23: Average flux through membrane over 24 hrs for sinusoidal membranes with different pattern height.

Weinman and Husson (2016) presented their experimental findings as flux over time. They presented the results for 120 mins for different membrane geometries. The simulation results of this study for 120 mins and experimental results from Weinman and Husson are presented in Figure 24. The flux decline trend in the model was similar to the experimental results. Although the difference between flat and patterned membrane is not very big.

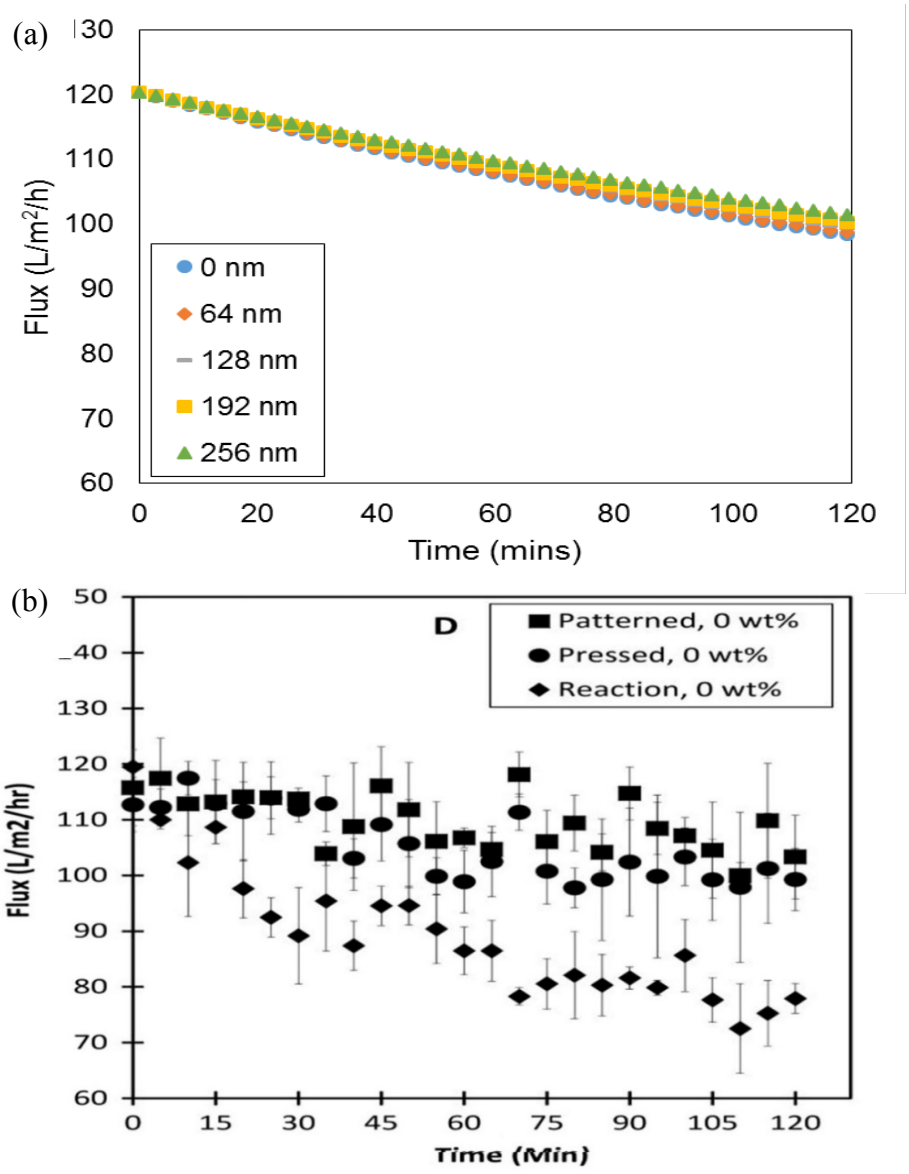

Figure 24: (a) Simulated and (b) experimental results for average flux through membrane over 120 mins (2hrs) for sinusoidal membrane geometries with different pattern height

4.2.1.4 Different K1 & K2 values

In the model, adsorption coefficient, k_1 and desorption coefficient, k_2 values play an important role to control the flux decline with time. So, by adjusting those values, the flux decline pattern from (Weinman and Husson 2016)'s experiment can be achieved. Different values of k_1 and k_2 were tried out to get the expected flux decline pattern. Several fitting exercises were done and some of the results for base case membrane are presented in Figure 25. Figure 25a shows the effect of changing k_1 values keeping k_2 fixed and Figure 25b shows effect of changing k_2 keeping k_1 fixed. Here, higher k_1 gives higher foulant adsorption and higher flux decline by comparing the flux decline trends in Figure 25 with Figure 24(b). The k_1 & k_2 values that give the similar trend with experimental data are 10^{-3} m^3/mol/s and 10^{-6} s^{-1} respectively.

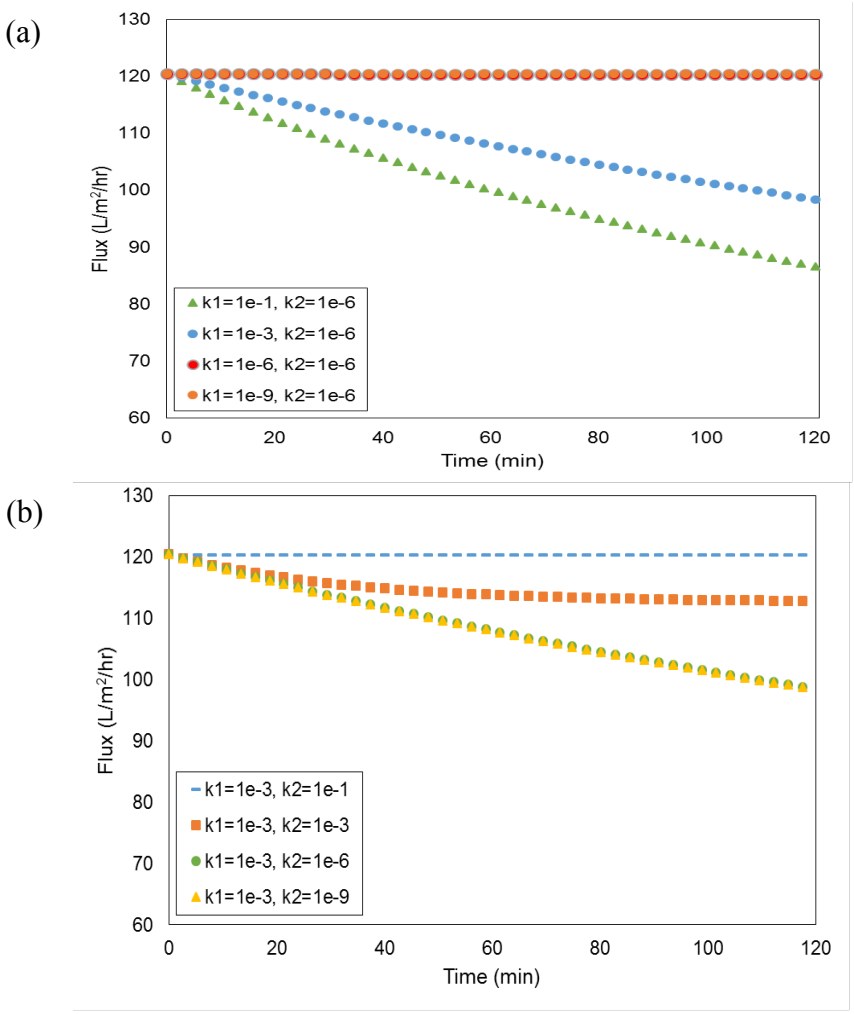

Figure 25: Change in flux decline trend in base case membranes with different (a)k_1 and (b) k_2 values

4.2.1.5 Change in F

According to Equation (6-7) the fouling coefficient (F) has a very big influence on the flux decline trend. This controls how the foulant accumulation on membrane surface affects the flux decline. Higher value of F gives faster flux decline and vice versa (Figure 26). In this study to achieve the trend in Figure 24(b), the value of F used was 2.5×10^{13} m/mol.

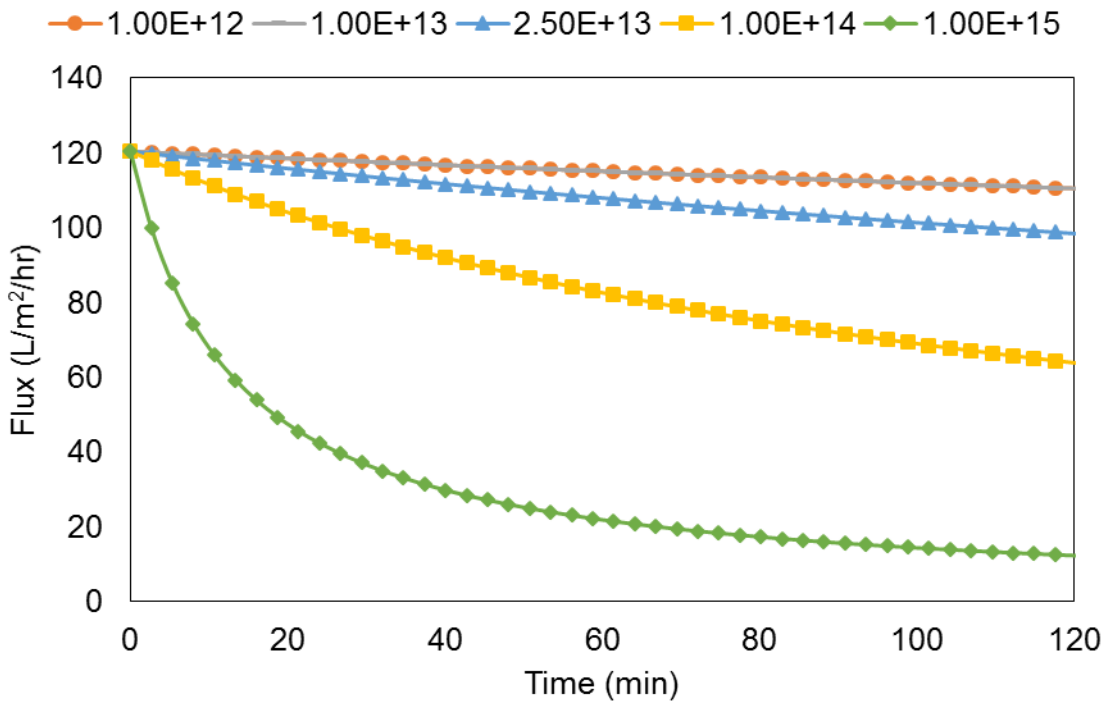

Figure 26: Change in flux decline trend in base case membrane with different F values

4.2.1.6 Effect of Inflow velocity

To examine the hydrodynamic effect on the adsorption process in LA approach, the base case model was simulated with different crossflow velocity. Though there were no hydrodynamic component in the Langmuir adsorption equation (Eq. 1), there are indirect effects of hydrodynamics on adsorption. When the crossflow velocity was higher, the adsorption process become faster and reached the equilibrium faster. The effect on changing inflow velocity is presented in Figure 27.

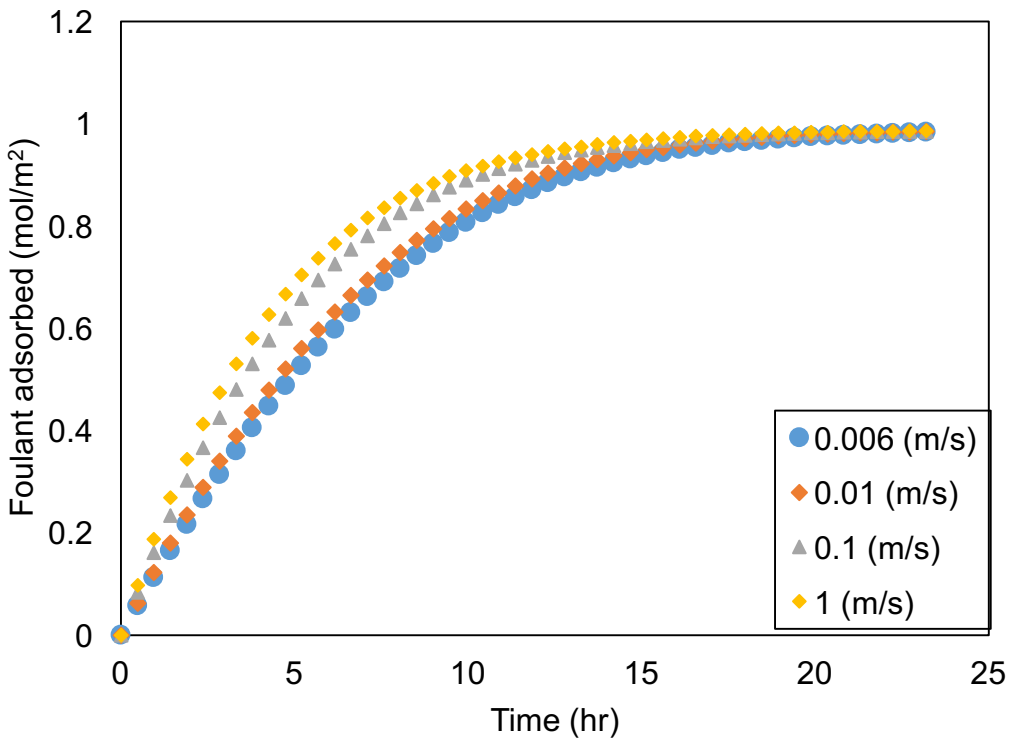

Figure 27: Effect of different inflow velocity on foulant accumulation on base case membrane surface.

4.2.2 Modified Langmuir Adsorption (MLA) approach

To incorporate shear effect on foulant accumulation on membrane surface, modified Langmuir equation (Eq. 6) has been used to obverse what difference can shear effect make in foulant adsorption.

4.2.2.1 Foulant accumulation on membrane surface

Figure 18 shows the shear over the membrane surface. Incorporating shear in desorption term in modified Langmuir equation, will consider the foulant accumulation much lower than the simulation that was done using Langmuir equation. Due to high shear in the peaks of the membrane pattern, it is expected to have much lower foulant accumulation on the peaks. For, MLA approach k_l was higher than the k_l used in LA approach. Figure 28 illustrates adsorbed foulant on membrane surface (left 2000nm) at time point 120mins. Here, 0 nm (flat) membrane did not have much varied foulant accumulation throughout the membrane surface. The figure shows that the foulant accumulation is less in peaks than in valleys. Higher the pattern of membrane and shear, lower the foulant accumulation on the peaks. But in the valleys, the opposite happens. As higher pattern

height makes bigger valleys with low shear, it helps to accumulate more foulant in valleys. The peaks in adsorbed foulant in Figure 28 represents the accumulated foulants in valleys. An interesting observation can be made in the curves for 192 nm and 256 nm. Instead of having a high peak in accumulated foulant in valleys, for this two patterns the peak is broken. The probable reason for this is the generation of high velocity streamlines and shear along peak of the membrane patterns. This prevents the development of precise peaks of in accumulated foulant in the valleys of patterned membranes with height 192nm and 256 nm.

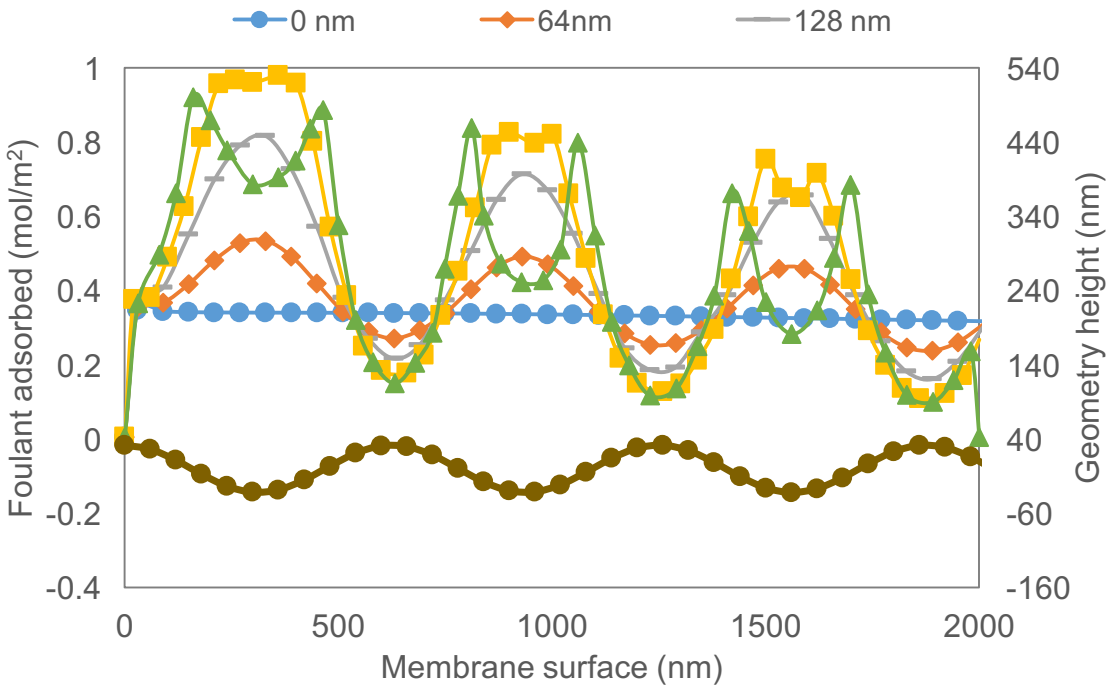

Figure 28: Foulant accumulation on membrane surface with effect of shear at a definite time point (120mins) for sinusoidal membranes with different pattern heights.

Despite having higher shear and lower concentration in peaks, average foulant accumulation on membrane surface over 24 hrs is higher for sinusoidal patterns with higher pattern height (Figure 29a). The reason behind is the higher foulant development in valleys. Also, because of the broken peaks in valleys, differences between the average foulant accumulation on membrane of different pattern heights are not consistent. Average foulant accumulation over time for first 2 hours is presented in Figure 29b. In first two hrs, the average foulant accumulation was higher in membranes with lower pattern.

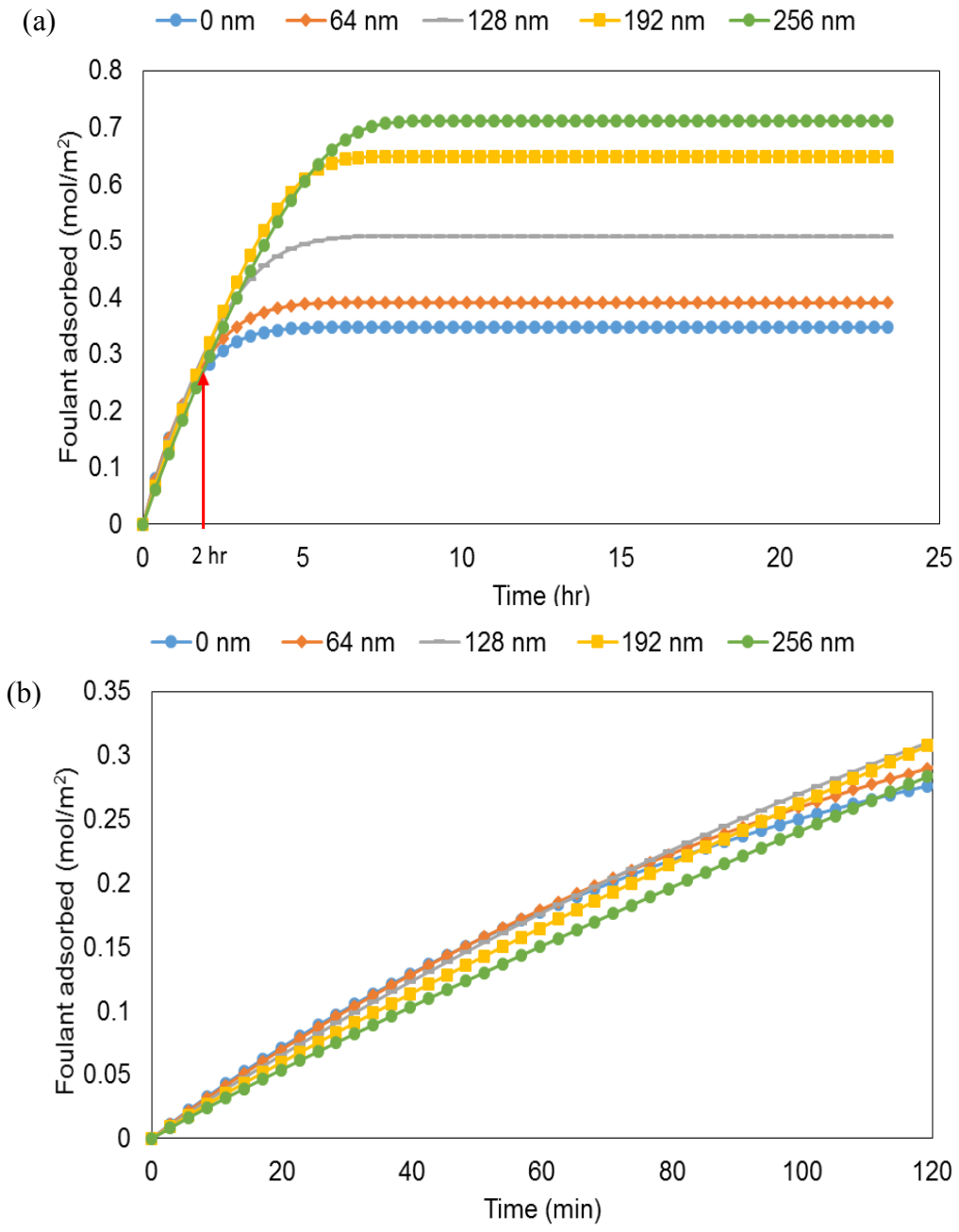

Figure 29: Average foulant accumulation on membrane surface with effect of shear with time for (a) 24 hrs (b) 2 hrs (120 mins) for sinusoidal membranes with different pattern heights.

4.2.2.2 Flux through the membranes

As high shear lets less foulant to adsorb onto membrane surface (Figure 28), flux through the peaks of patterned membranes is more than in valleys. Higher membrane pattern gives higher flux around

the peaks (Figure 30). At the same time, larger amount of foulant accumulates in bigger valleys that exist in higher pattern geometry. So, the average accumulated foulant is higher and average flux is lower in membranes with bigger pattern height (

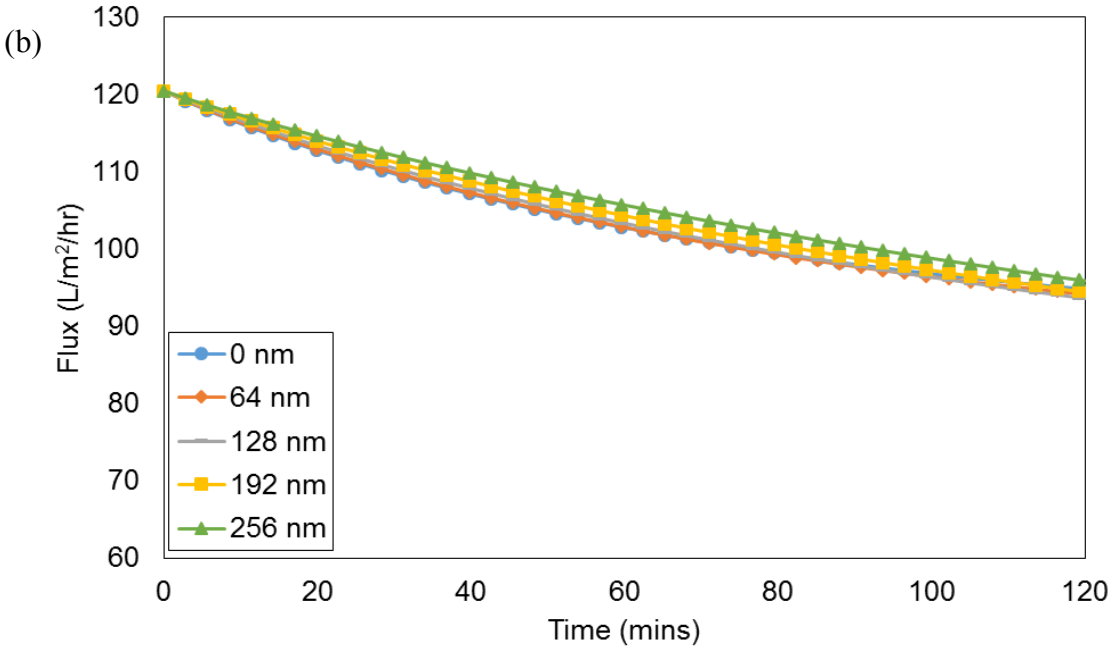

Figure 31).

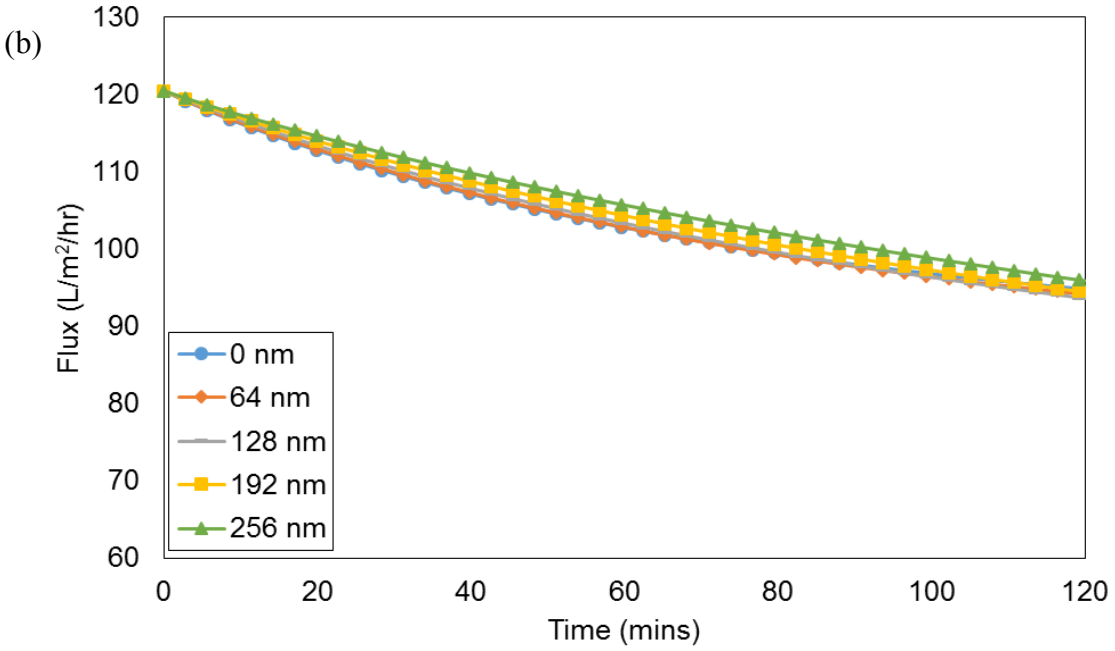

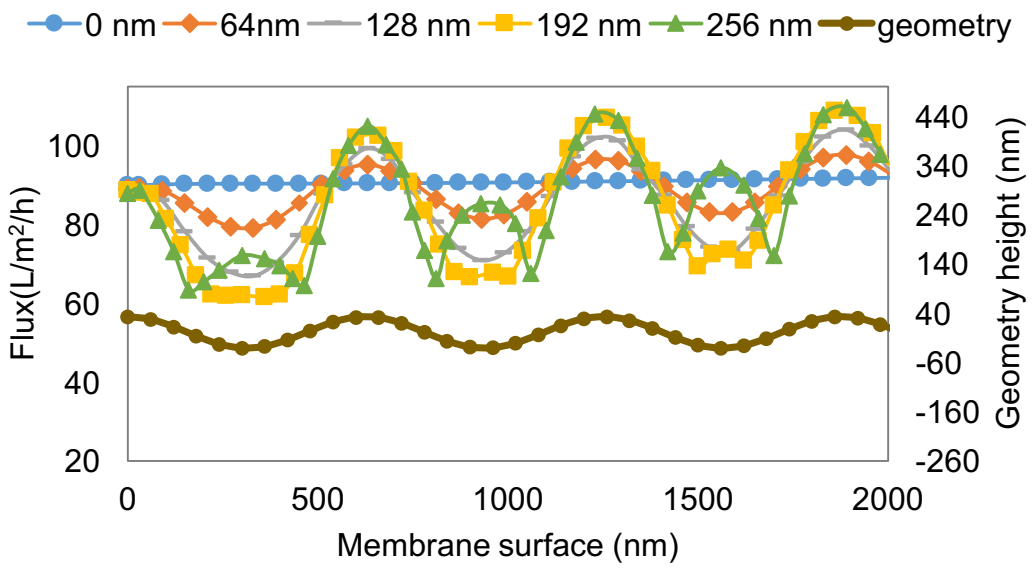

Figure 30: Flux through membrane surface with effect of shear at a definite time point (120mins) for sinusoidal membranes with different pattern heights.

(a)

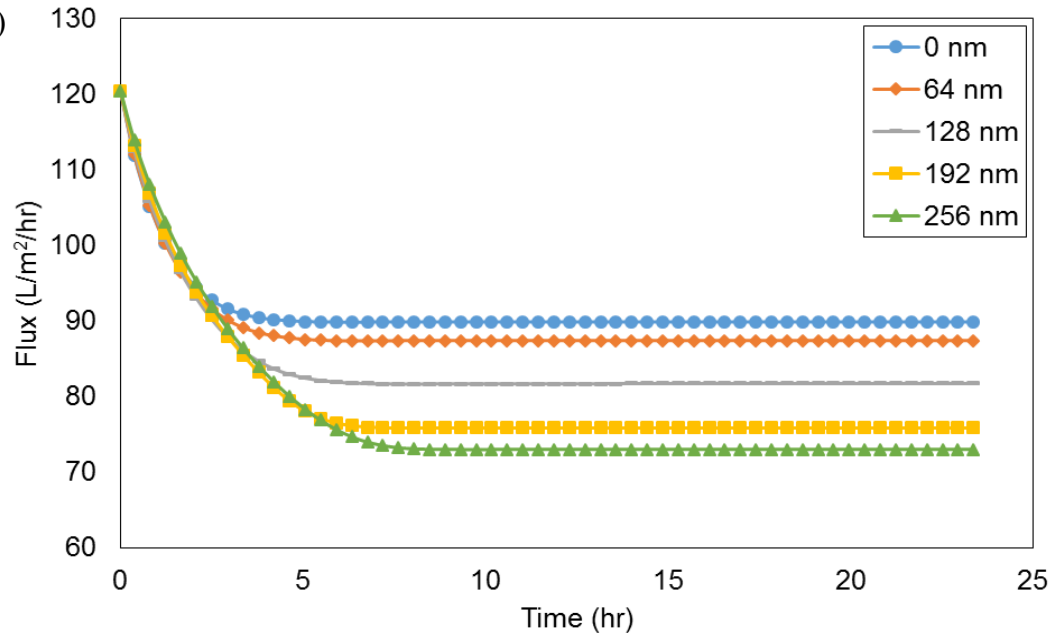

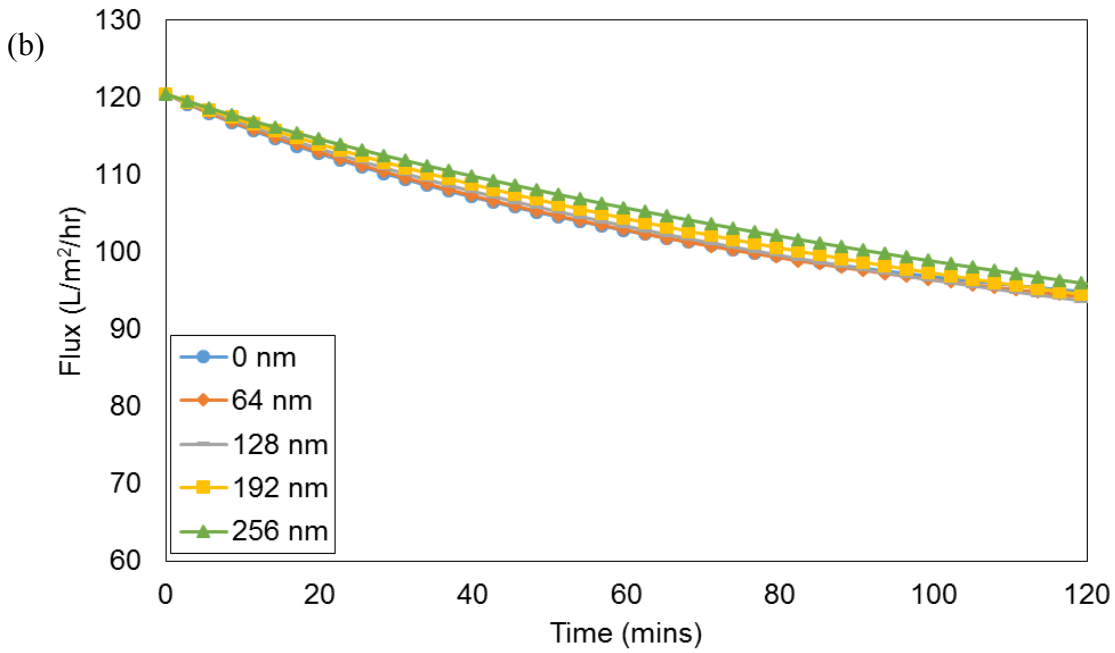

Figure 31: Average flux through membrane with effect of shear with time for (a) 24 hrs (b) 2 hrs (120 mins) for sinusoidal membranes with different pattern heights.

4.2.2.3 Different K1 & K2 values

Modifying Langmuir equation by incorporating shear term, changed the required k_1 and k_2 values to generate the flux decline trend in (Weinman and Husson 2016)'s work (Figure 24b). In MLA approach the desorption is much higher than adsorption compared to LA approach. So, to achieve same trend in average flux decline in MLA approach and Figure 24b , fitting exercises were performed and the values of k_1 and k_2 are adjusted again. Some of the fitting exercise results in base case membrane are presented in Figure 32. By comparing Figure 32 and Figure 24b, the chosen k_1 and k_2 values were 10^{-1} m^3/mol/s and 10^{-6} (-). It should be noted that multiplying shear rate to the desorption term changed the unit of of k_2.

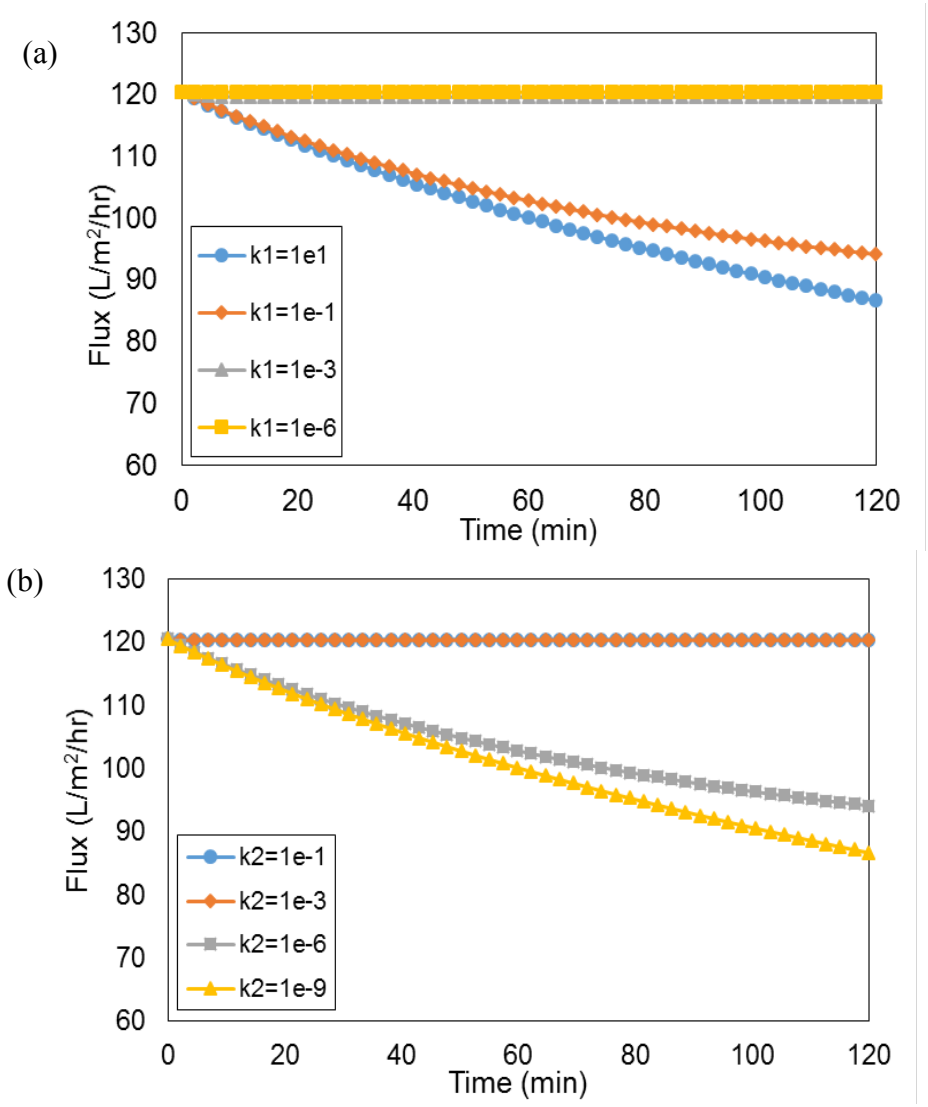

Figure 32: Change in flux decline trend for base case membrane with different (a)k_1 and (b) k_2 values

After increasing k_1 from 10^{-3} m^3/mol/s to 10^{-1} m^3/mol/s, the adsorption rate becomes higher than LA approach and average flux become similar in both approaches. This happens because of higher amount of foulant accumulation in valleys of the membranes at same time point.

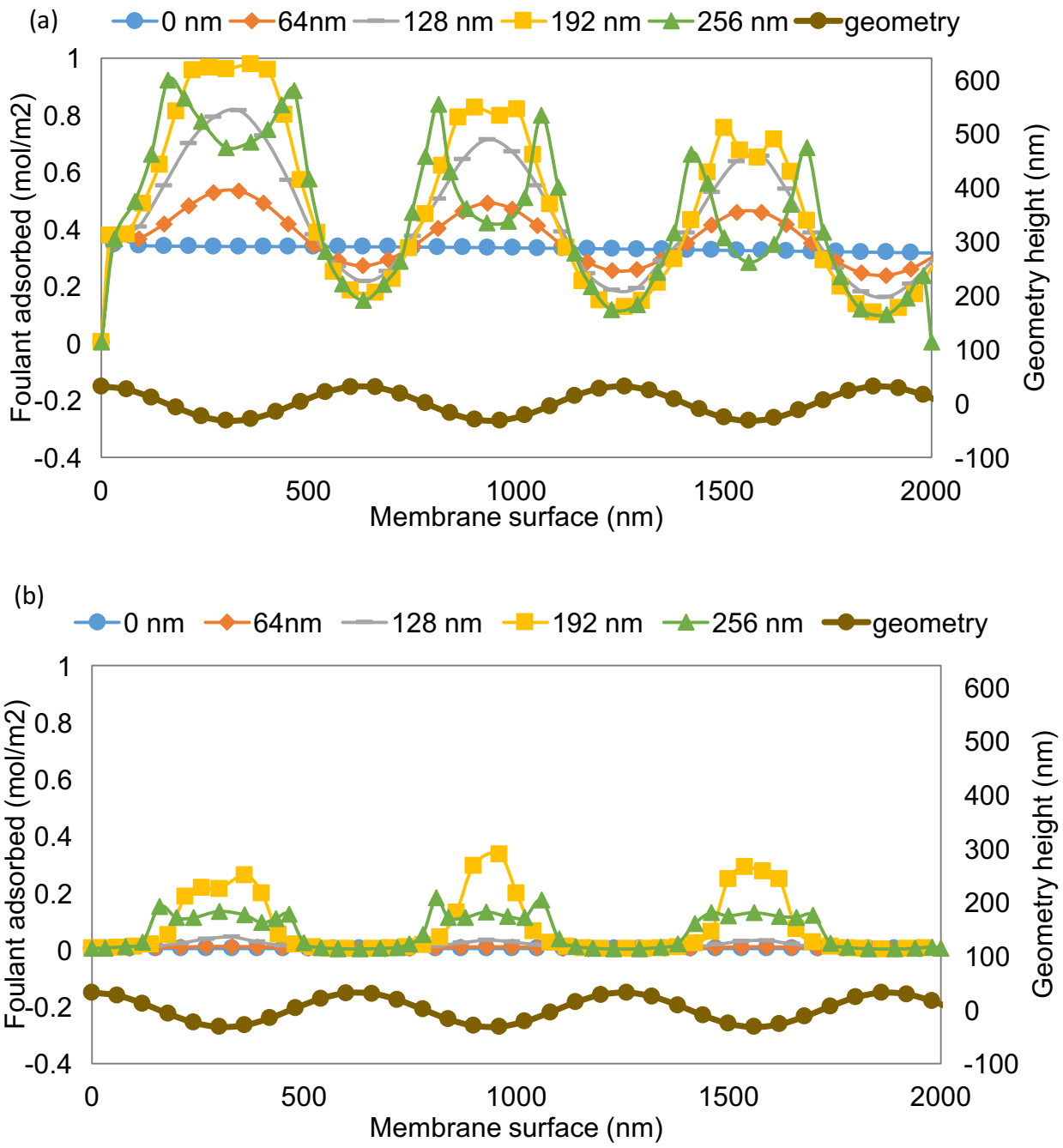

Figure 33: Accumulated foulnt on membrane surface after 120 mins for (a) $k_1 = 10^{-1}$ $m^3/mol/s$, $k_2 = 10^{-6}$ (b) $k_1 = 10^{-3} m^3/mol/s$, $k_2 = 10^{-6}$

4.2.2.4 Change in F

Besides k_1 and k_2, value of F is also required to be checked for MLA Approach. Some of the fitting exercise results are presented in Figure 34. It seemed to work with the same value of F (2.5×10^{13}) as in LA approach for k_1 and k_2 10^{-1} m^3/mol/s and 10^{-6} (-) respectively.

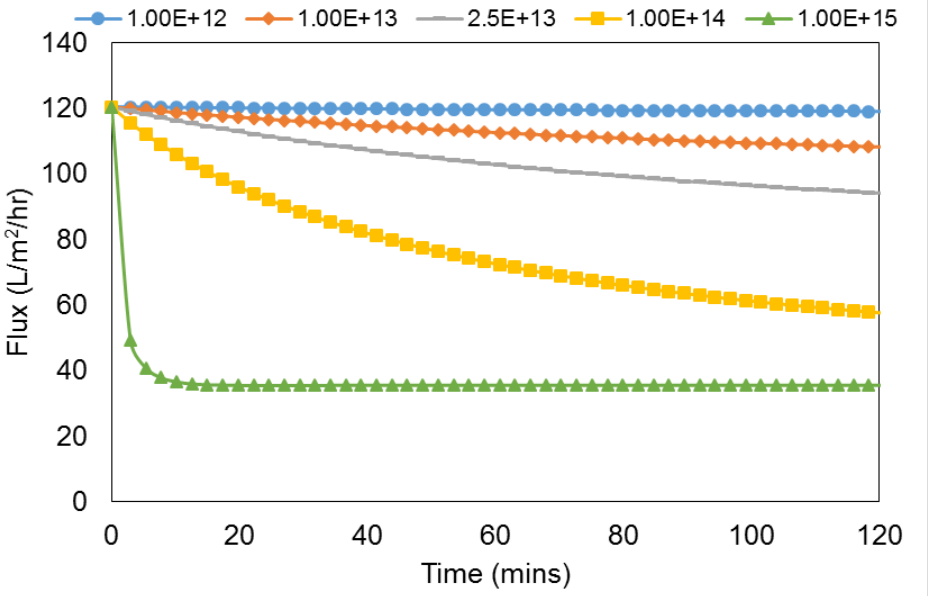

Figure 34: Change in flux decline trend with different F values in base case membrane for MLA approach

4.3 Foulant transport and adsorption for alternative pattern geometries

4.3.1 Random surface roughness

5 different membranes were constructed by generating random patterns with 5 different highest pattern height (Figure 9).

Figure 35 shows the corresponding shear profiles. Foulant transport and adsorption on membranes with random roughness were calculated using MLA approach (Eq 6) and presented in Figure 36 for both 24 hrs and 2 hrs (120 mins).

The foulant accumulation (Figure 36) and flux decline (Figure 37) in random roughness membranes show almost similar trend as sinusoidal patterned membranes (Figure 29) (

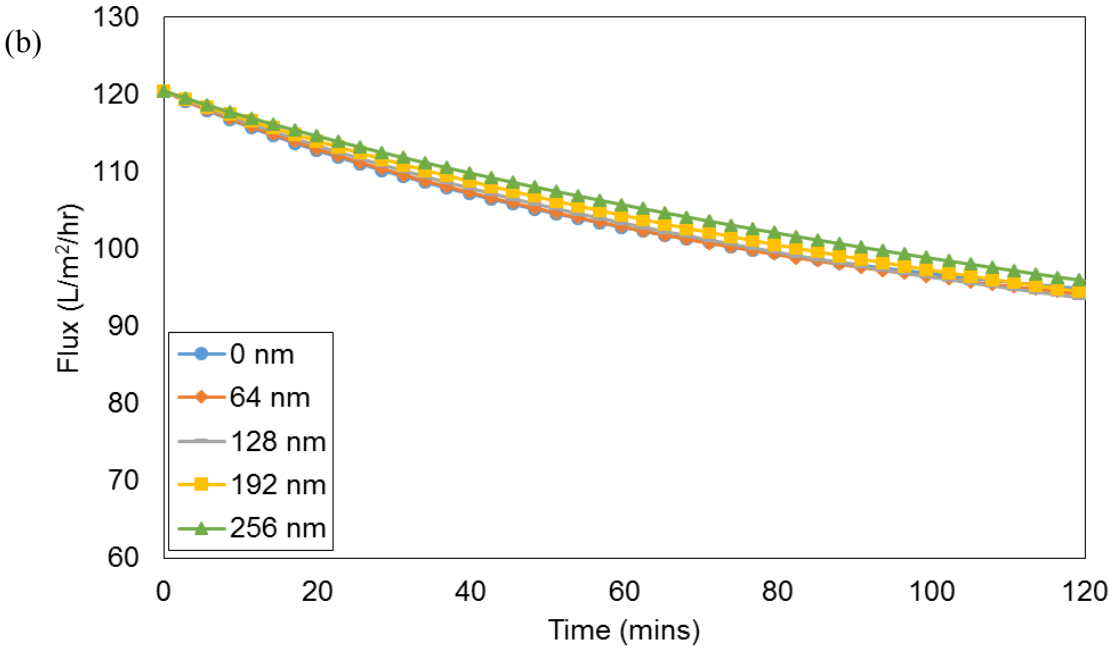

Figure 31). The average adsorbed foulant on membrane surface was higher and average flux was lower for membranes with higher pattern height

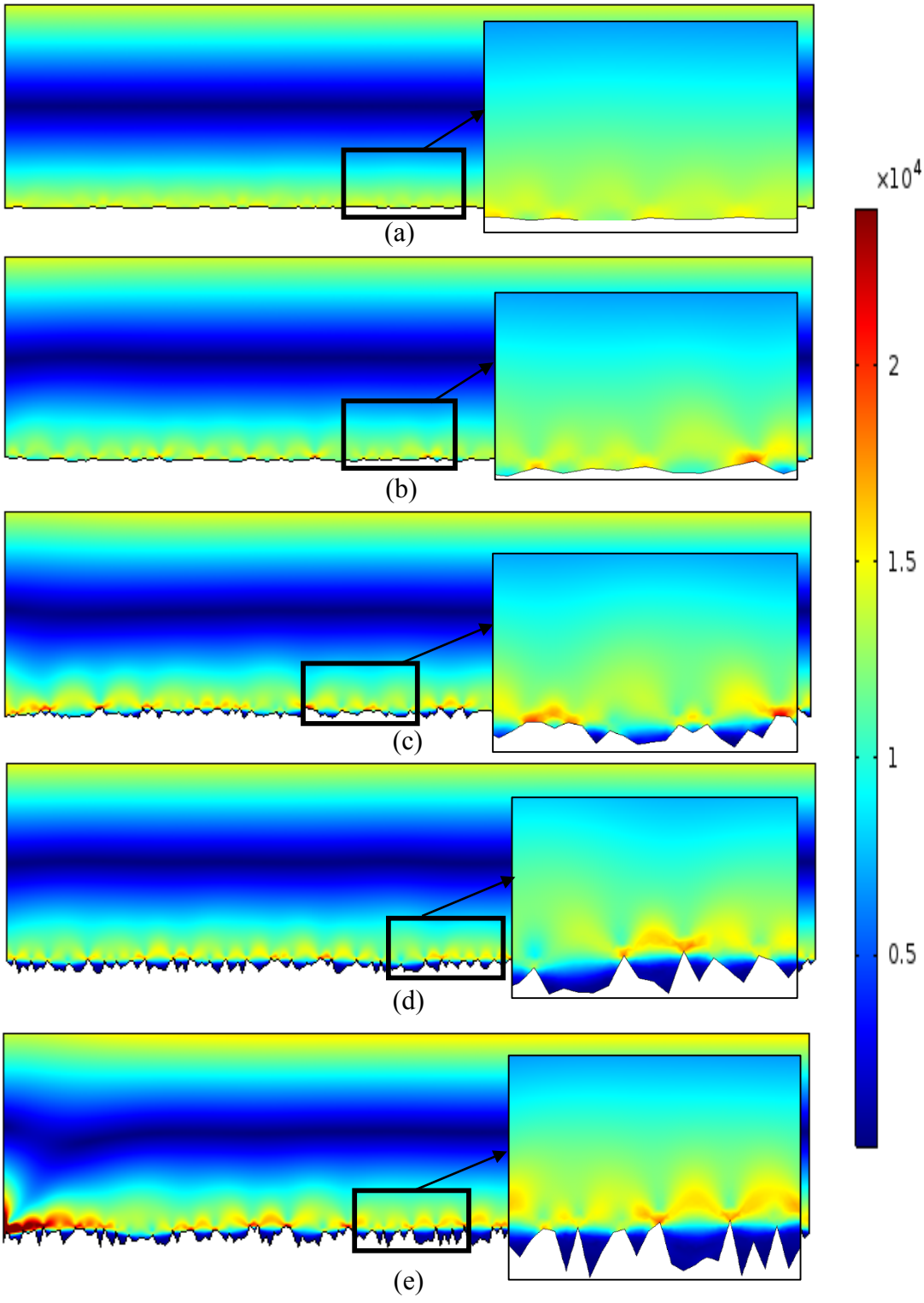

Figure 35: shear profile of membrane geometries with random roughness comparable to sinusoidal membranes with pattern height (a) 0 nm, (b) 64 nm, (c) 128 nm, (d) 192 nm and (e) 256 nm

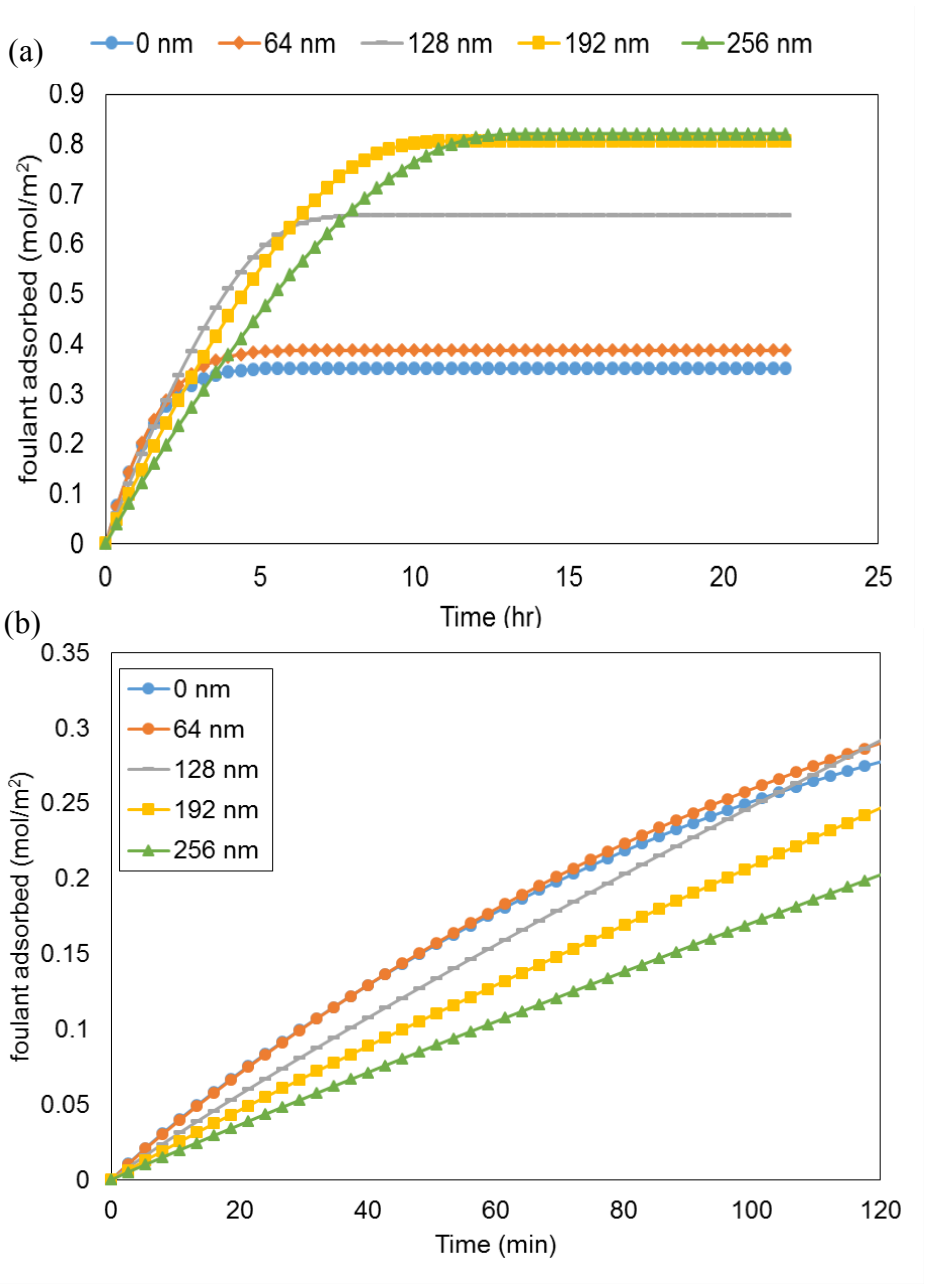

Figure 36: Average foulant accumulation on membrane surface with effect of shear with time for (a) 24 hrs and (b) 120 mins for membranes with random roughness comparable to sinusoidal membranes with pattern height 0 nm, 64 nm, 128 nm, 192 nm and 256 nm.

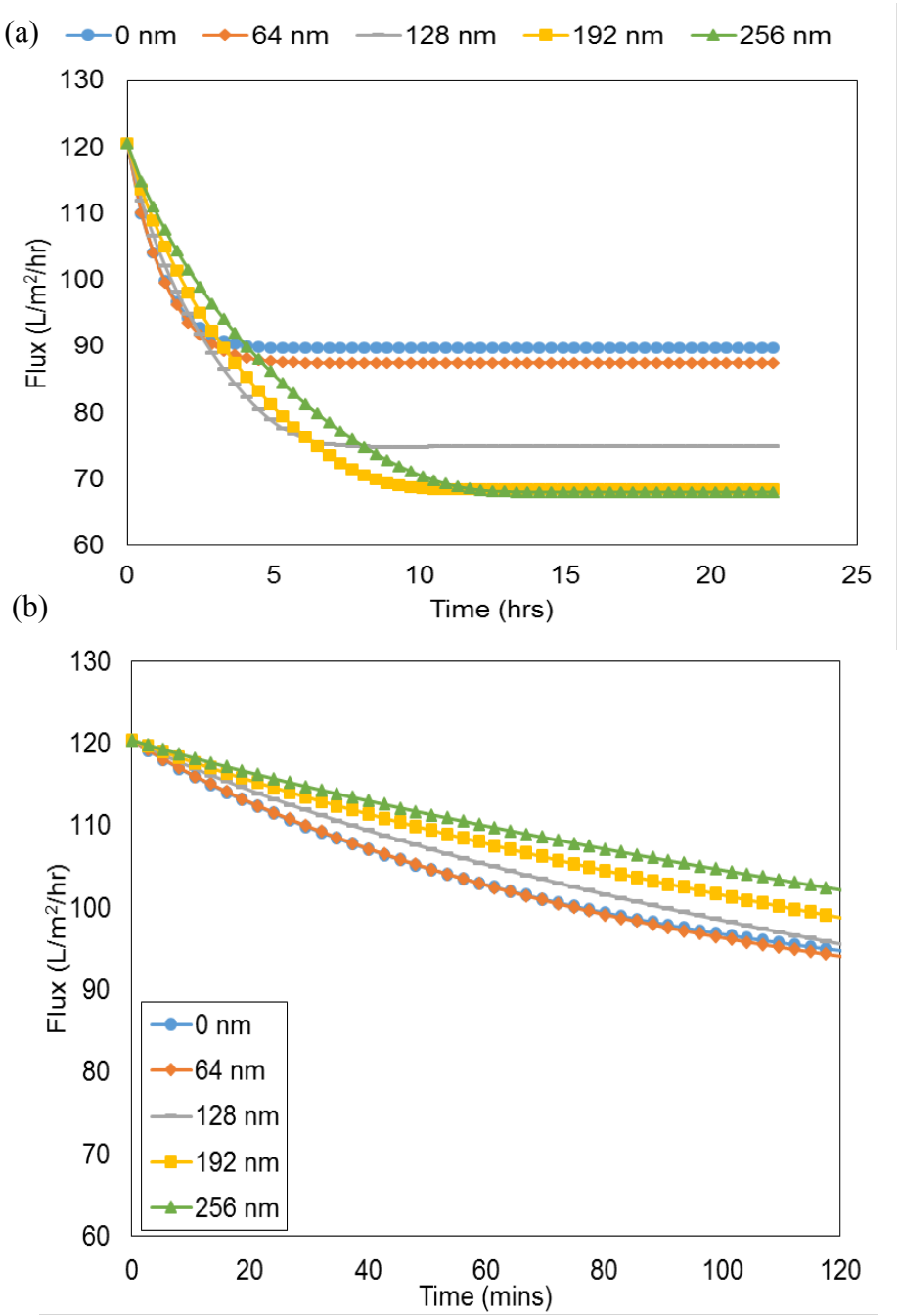

Figure 37: Average flux through membrane with effect of shear with time for (a) 24 hrs and (b) 120 mins for membranes with random roughness comparable to sinusoidal membranes with pattern height 0 nm, 64 nm, 128 nm, 192 nm and 256 nm.

To make direct comparison, percentage of flux decline in 24hrs for both random roughness membrane and sinusoidal membranes are plotted in Figure 38. For both kind of membranes, flux decline increased for higher pattern height. Also, sinusoidal membranes mostly maintained lower flux decline than random roughness membrane. Higher the pattern height gets, more visible the differences in flux decline between two kinds of membranes become. This indicates more foulants accumulate in membranes with random roughness than in membranes with sinusoidal patterns with.

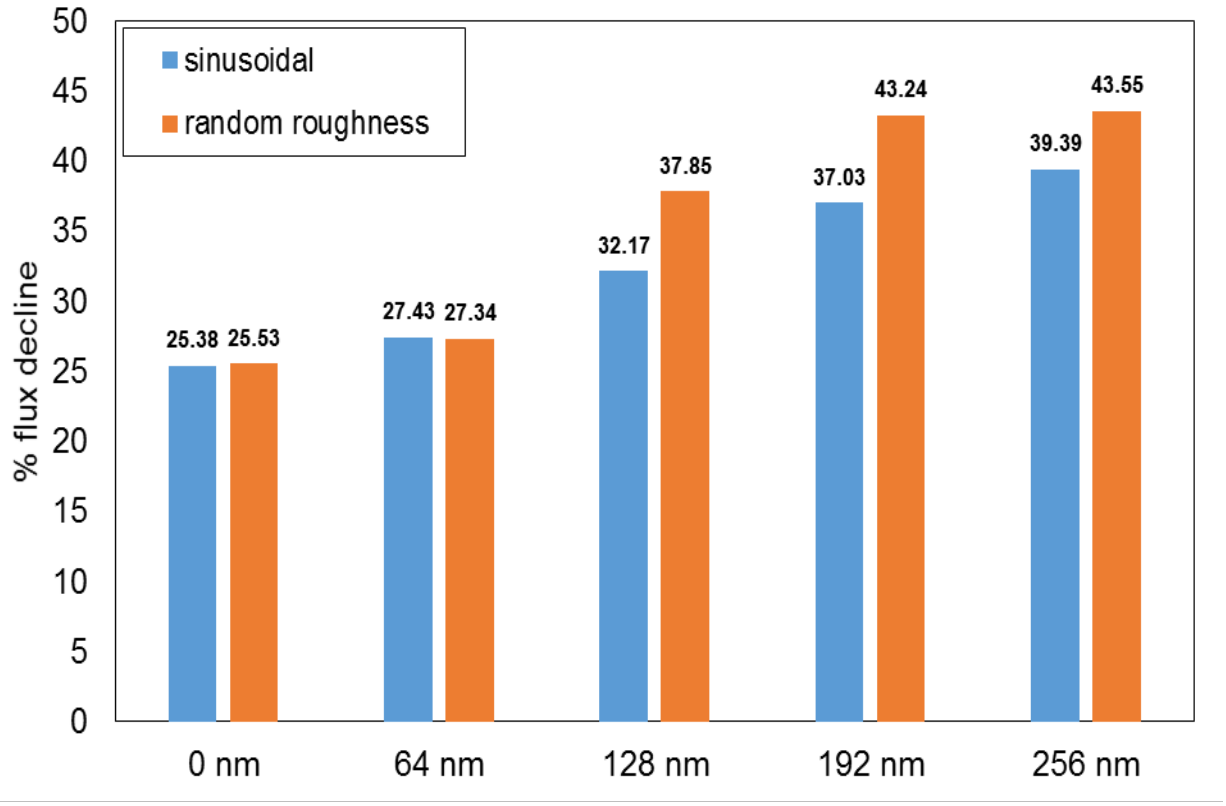

Figure 38: Comparison of percentage of flux decline after 24 hrs for membranes with random roughness to sinusoidal patterned membranes.

4.3.2 Other geometrical patterns

As seen in Figure 28, less fouling can only be achieved near the peaks of sinusoidal membrane patterns. But because of the existence of deep valleys, more foulant accumulates there compared to the amount of foulant that gets removed due to shear. So, if a geometry that has shallower valleys can give better results.

The velocity profile shows that the valleys are more associable to the water stream in trapezoidal and triangular than in sinusoidal patterned membrane (Figure 39). The shear profiles show that because of having shallower valleys than sinusoidal patterned membrane, trapezoidal and triangular patterns have higher shear in valley Figure 41. Also, for triangular pattern there is no base like trapezoidal pattern which lets less foulant accumulate on membrane surface by giving higher shear (Figure 40Figure 41).

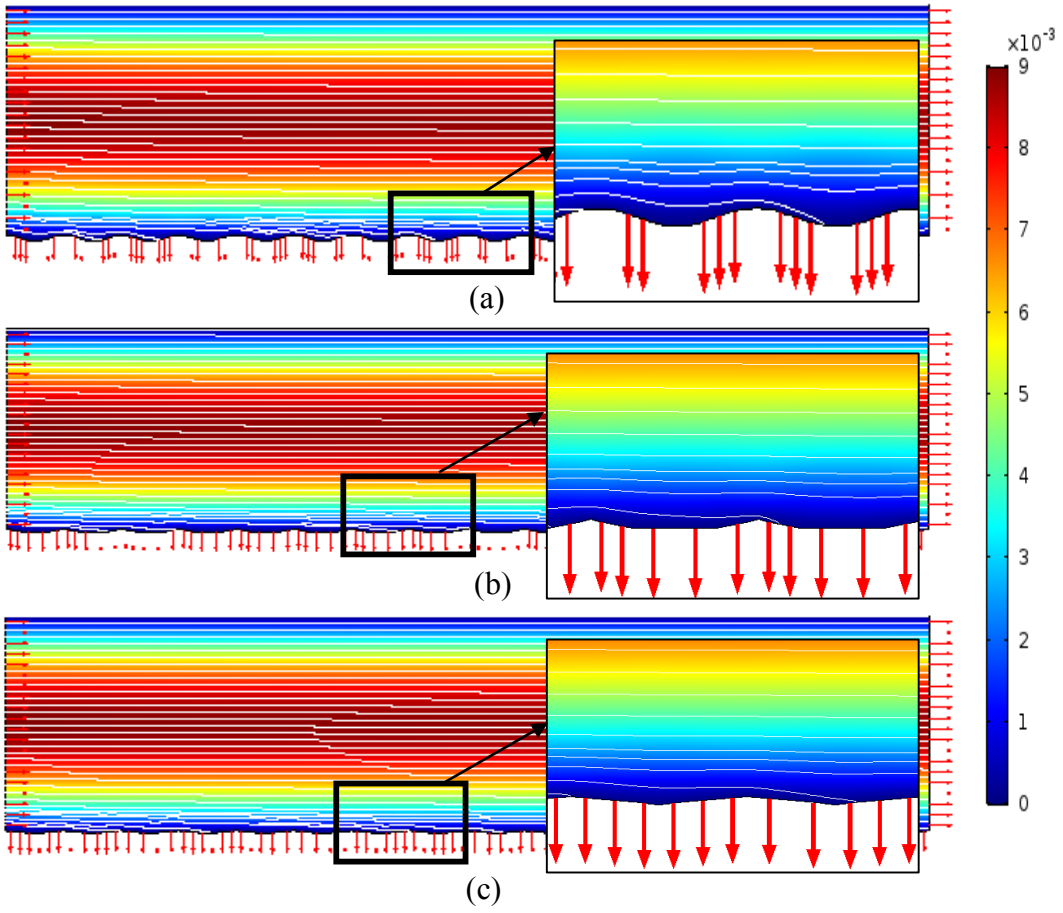

Figure 39: Velocity profiles of membrane geometries with (a) sinusoidal pattern (64 nm) (b) trapezoidal pattern and (c) triangular pattern.

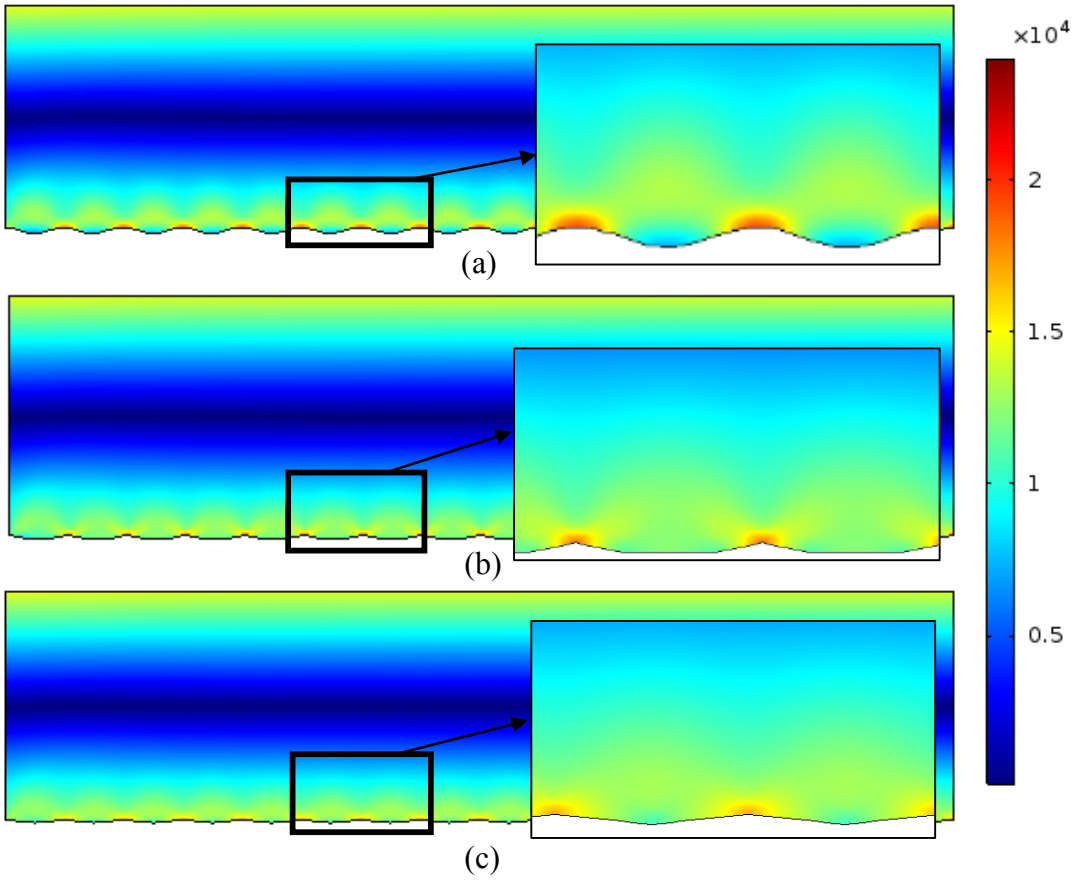

Figure 40: Shear profiles of membrane geometries with (a) sinusoidal pattern (64 nm) (b) trapezoidal pattern and (c) triangular pattern.

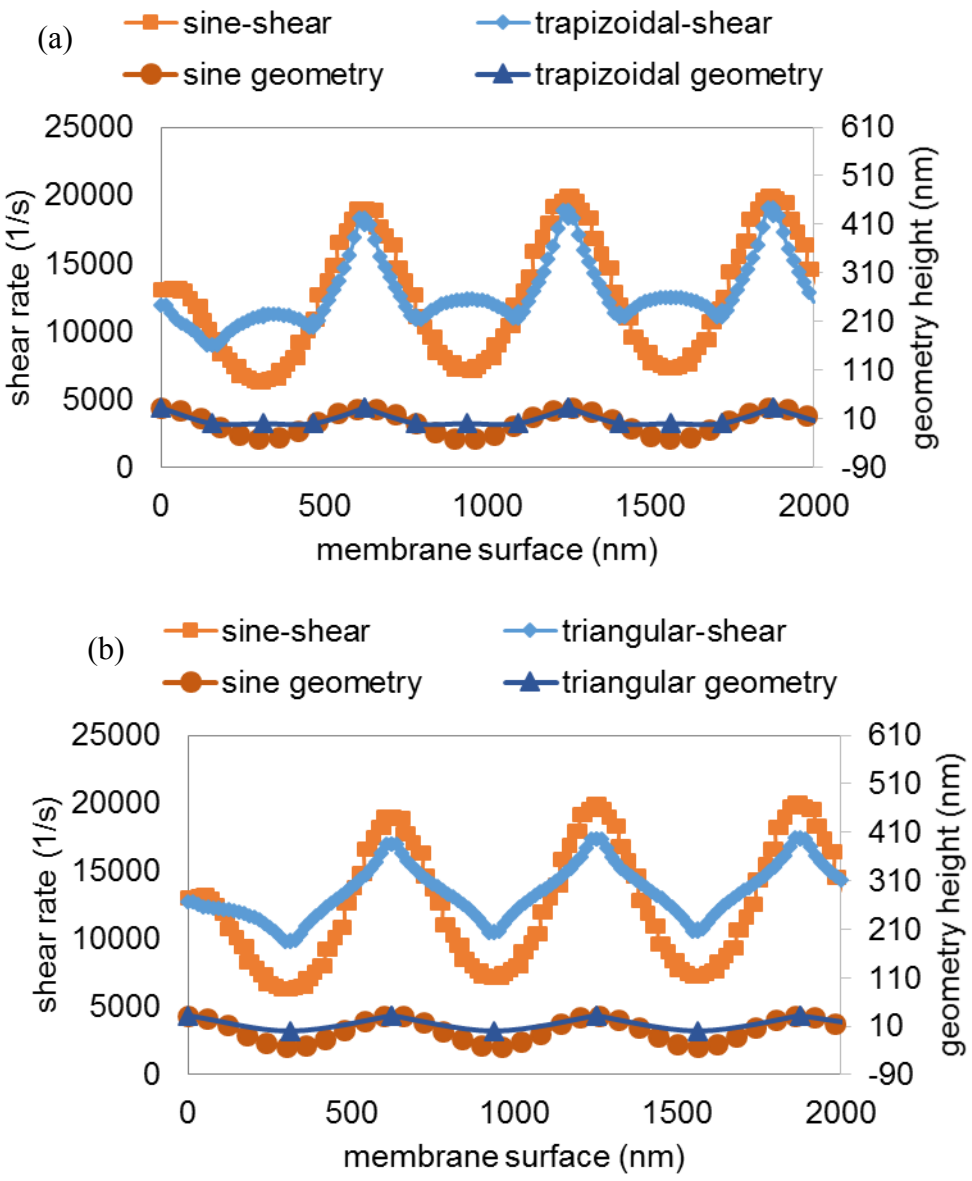

Figure 41: Comparison of shear on membrane surface of (a) sinusoidal and trapizoidal patterned membrane and (b)sinusoidal and triangular patterned membrane

Average flux through membrane over time for trapezoidal and triangular patterned membrane was compared to the average flux of sinusoidal (base case) patterned membrane (Figure 42). The comparison shows that the difference in flux yield is not very big in three geometries in 120 mins. Sinusoidal membrane has comparatively the lower flux yield. Percentage of flux decline in Figure

43 also shows the lowest % flux decline for triangular patterned membrane and 64 nm sinusoidal patterned membrane show the highest.

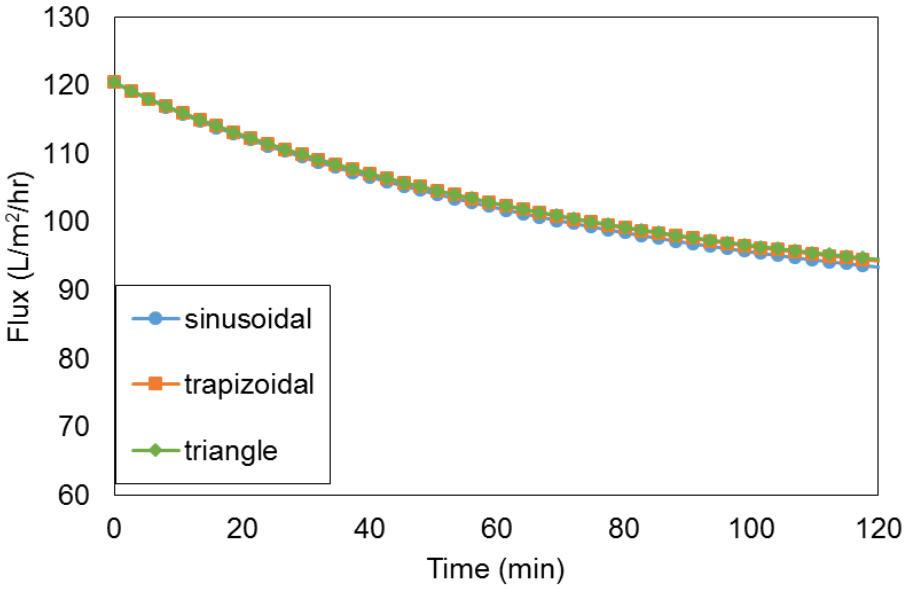

Figure 42: Average flux through membrane with effect of shear with time (120 mins) for different patterned membranes.

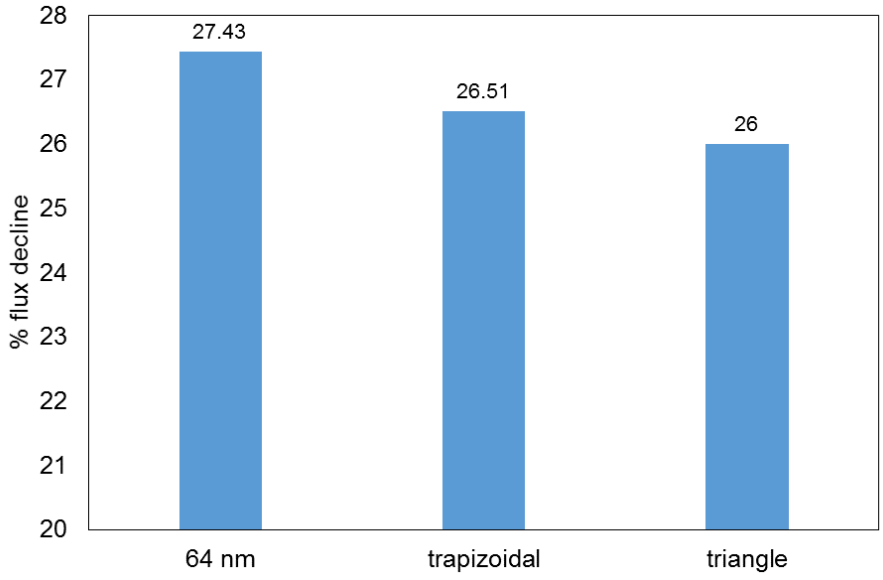

Figure 43: Percentage of flux decline through membrane with effect of shear with time (120 mins) for different patterned membranes

5 Other efforts

Some other efforts were approached during this study but were not pursued further due to convergence limitation.

5.1 Additional Shear Term

In the MLA approach (Eq 6) that has been discussed in section 4.2.2, the shear rate was multiplied to the desorption term of Langmuir equation to incorporate direct shear effect on adsorption. Another effort for modification of Langmuir adsorption equation was equation 10.

$$\frac{dC_s}{dt} = K_1 C(C_{se} - C_s) - K_2 C_s - R_s \tag{8}$$

$$R_s = k_3 c_s \tau \tag{9}$$

Here, R_s is the shear term and k_3 is shear coefficient. This shear tern adds to desorption term to include the effect of shear to desorption.

But this effort for modification was unsuccessful because the simulation became complicated and almost impossible to converge the model to have successful results. The model only converged and was able to give solution for only very small values of k_3 which made R_s term so small that it had hardly any effect on adsorption. The effect of shear was hardly seen.

5.2 One Step Study

To construct simpler model and make simulations easier, the hydrodynamics and foulant adsorption equations were combined and incorporated to a one step steady state model. Like it is explained in section 3.2.1, instead of using the equation (3), equation (6) was used which directly calculates flux after considering adsorbed foulant (c_s) on membrane surface. The model calculated c_s using the equation (12) which was derived from Modified Langmuir adsorption equation (Eq. 5) considering steady state.

$$c_s = \frac{1000 * k_1 * c}{k_1 * c + k_2 * \tau} \tag{10}$$

But the major problem with this effort also was convergence. The components of the equations were inter-dependent. It became very difficult to get the desired trend in hydrodynamics and flux output as the model converged for limited number of values of K_1, K_2 and F.

6 Future work

6.1 Particle tracing

The model was completely an adsorption model in this study. So foulant accumulation on membrane surface solely dependent on the defined adsorption equation and foulant was considered here as concentration. To evaluate the foulant particle interaction with membrane surface, the next step should be particle tracing approach. Here, foulants are considered as particles with definite diameter and number of foulant particles that enters the system can be defined. Depending on the hydrodynamic conditions the particles will flow through the system. While flowing through it can interact to the obstructions that it encounters on its way and depending on hydrodynamics it can get stuck or flow by. This approach will help to understand precisely how can foulants get removed, how much area gets covered by foulant and what are the effects of changing membrane structures.

6.2 Turbulent Modelling

In this study the flow was considered as Laminar flow. Although the parameters for the model were taken from Weinman and Husson's work (Weinman and Husson 2016) and the crossflow velocity they used was 1 m/s. It was downscaled for this study. But the next modelling step can be defining the flow behavior as turbulent flow.

6.3 Effect of concentration polarization

Effect of concentration polarization is not simulated in this study. So, to include that, change of boundary conditions like flux yield through membrane and adding salt concentration can be considered. Also, as described in 6.1, Particle tracing also a good way to simulate membrane filtration system with concentration polarization.

6.4 3D modeling

For this study, the simulated geometries were 2D. Converting these models to 3D can be a good way to have simulation results which agree more to the practical data.

6 Conclusion

CFD Simulations illustrated two approaches with indirect (LA) and direct (MLA) effect of hydrodynamics during adsorption. Simulation showed that with LA approach higher sinusoidal patterns accumulate less amount of foulant and flux decline on membrane surface. But the differences between sinusoidal pattern height needs to be significant to have a noticeable change. LA approach was able to show the similar trend in flux decline for both membranes with 0 nm and 64nm (base case) pattern height in simulated and experimental data of Weinman and Husson (Weinman and Husson 2016) (Figure 24b).. The difference between average fluxes for these two membranes were very small in both cases. But in LA approach the foulant accumulation was high is peaks and low in valleys. This shows that this approach does not consider any shear stress that is caused by water stream in the system. Also, sinusoidal membranes with higher patterns were showing less fouling because of bigger surface area than a membrane with smaller sinusoidal pattern height.

MLA approach had direct effect of hydrodynamics and it showed shear can play a big role in fouling mitigation in patterned membranes. Higher sinusoidal patterned membranes had higher shear along their peaks which kept the flux high in that area. But it was also seen that, because of more foulant accumulation in valleys of membranes with higher sinusoidal pattern height, the average calculated foulant accumulation and flux decline was higher with time compared to the membranes with smaller pattern height.

Membranes with random roughness were seen to have higher foulant accumulation and flux decline with time compared to sinusoidal patterned membranes when simulated using MLA approach. But, trapezoidal and triangular patterns with same period and half of the pattern height of sinusoidal base case membrane were seen to accumulate less foulant and have less flux decline.

8 References

Al-Amoudi, Ahmed, and Robert W. Lovitt. 2007. “Fouling Strategies and the Cleaning System of NF Membranes and Factors Affecting Cleaning Efficiency.” *Journal of Membrane Science* 303 (1): 4–28. doi:10.1016/j.memsci.2007.06.002.

Al-Amoudi, Ahmed Saleh. 2010. “Factors Affecting Natural Organic Matter (NOM) and Scaling Fouling in NF Membranes: A Review.” *Desalination* 259 (1): 1–10. doi:10.1016/j.desal.2010.04.003.

Bellona, Christopher, Jog E Drewes, Pei Xu, and Gary Amy. 2004. “Factors Affecting the Rejection of Organic Solutes during NF/RO Treatment—a Literature Review ARTICLE IN PRESS.” *Water Research* 38: 2795–2809. doi:10.1016/j.watres.2004.03.034.

Bikel, Matías, Ineke G. M. Pünt, Rob G. H. Lammertink, and Matthias Wessling. 2009. “Micropatterned Polymer Films by Vapor-Induced Phase Separation Using Permeable Molds.” *ACS Applied Materials & Interfaces* 1 (12). American Chemical Society: 2856–61. doi:10.1021/am900594p.

Bowen, W.Richard, Teodora A. Doneva, and H.B. Yin. 2002. “Atomic Force Microscopy Studies of Membrane—solute Interactions (Fouling).” *Desalination* 146 (1–3): 97–102. doi:10.1016/S0011-9164(02)00496-4.

Cheryan, Munir., and Munir. Cheryan. 1998. *Ultrafiltration and Microfiltration Handbook*. Technomic Pub. Co.

Chou, Stephen Y. 1996. “Nanoimprint Lithography.” *Journal of Vacuum Science & Technology B: Microelectronics and Nanometer Structures* 14 (6): 4129. doi:10.1116/1.588605.

Clark, Mark M. 2009. *Transport Modeling for Environmental Engineers and Scientists*. Wiley. http://www.wiley.com/WileyCDA/WileyTitle/productCd-0470260726,subjectCd-CH22.html.

Comsol. 2016. “Detailed Explanation of the Finite Element Method (FEM).” *Comsol Website*. https://www.comsol.com/multiphysics/finite-element-method.

Çulfaz, P. Zeynep, Steffen Buetehorn, Lavinia Utiu, Markus Kueppers, Bernhard Bluemich, Thomas Melin, Matthias Wessling, and Rob G. H. Lammertink. 2011. "Fouling Behavior of Microstructured Hollow Fiber Membranes in Dead-End Filtrations: Critical Flux Determination and NMR Imaging of Particle Deposition." *Langmuir* 27 (5). American Chemical Society: 1643–52. doi:10.1021/la1037734.

Demneh, Seyedeh Marzieh Ghasemi, Bahram Nasernejad, and Hamid Modarres. 2011. "Modeling Investigation of Membrane Biofouling Phenomena by Considering the Adsorption of Protein, Polysaccharide and Humic Acid." *Colloids and Surfaces B: Biointerfaces* 88 (1): 108–14. doi:10.1016/j.colsurfb.2011.06.018.

Ding, Yifu, Sajjad Maruf, Masoud Aghajani, and Alan R. Greenberg. 2016a. "Surface Patterning of Polymeric Membranes and Its Effect on Antifouling Characteristics." *Separation Science and Technology* 6395 (July): 1–18. doi:10.1080/01496395.2016.1201115.

———. 2016b. "Surface Patterning of Polymeric Membranes and Its Effect on Antifouling Characteristics." *Separation Science and Technology* 6395 (July): 01496395.2016.1201115. doi:10.1080/01496395.2016.1201115.

Ding, Yifu, Jirun Sun, Hyun Wook Ro, Zhen Wang, Jing Zhou, Nancy J. Lin, Marcus T. Cicerone, Christopher L. Soles, and Sheng Lin-Gibson. 2011. "Thermodynamic Underpinnings of Cell Alignment on Controlled Topographies." *Advanced Materials* 23 (3). WILEY-VCH Verlag: 421–25. doi:10.1002/adma.201001757.

Drewes, J, and P Fox. 1999. "Fate of Natural Organic Matter (NOM) during Ground Water Recharge Using Reclaimed Water." *Water Science and Technology* 40 (9). IWA Publishing: 241–48. doi:10.1016/S0273-1223(99)00662-9.

Feng, X. J., and L. Jiang. 2006. "Design and Creation of Superwetting/Antiwetting Surfaces." *Advanced Materials* 18 (23). WILEY-VCH Verlag: 3063–78. doi:10.1002/adma.200501961.

Frei, Walter. 2013. "Meshing Considerations for Linear Static Problems | COMSOL Blog." *Comsol Blog*. https://www.comsol.com/blogs/meshing-considerations-linear-static-problems/.

Gença, Y., E. N. Durmaz, and P. Z. Çulfaz-Emecen. 2015. "Preparation of Patterned Microfiltration Membranes and Their Performance in Crossflow Yeast Filtration." *Journal of Membrane Science* 476: 224–33. doi:10.1016/j.memsci.2014.11.041.

Gironès, M., I.J. Akbarsyah, W. Nijdam, C.J.M. van Rijn, H.V. Jansen, R.G.H. Lammertink, and M. Wessling. 2006. "Polymeric Microsieves Produced by Phase Separation Micromolding." *Journal of Membrane Science* 283 (1): 411–24. doi:10.1016/j.memsci.2006.07.016.

Guo, L. J. 2007. "Nanoimprint Lithography: Methods and Material Requirements." *Advanced Materials* 19 (4). WILEY-VCH Verlag: 495–513. doi:10.1002/adma.200600882.

Ho, W. S. Winston, and Kamalesh K. Sirkar. 1992. "Overview." In *Membrane Handbook*, 3–15. Boston, MA: Springer US. doi:10.1007/978-1-4615-3548-5_1.

Jang, Jun Hee, Jaewoo Lee, Seon Yeop Jung, Dong Chan Choi, Young June Won, Kyung Hyun Ahn, Pyung Kyu Park, and Chung Hak Lee. 2015. "Correlation between Particle Deposition and the Size Ratio of Particles to Patterns in Nano- and Micro-Patterned Membrane Filtration Systems." *Separation and Purification Technology* 156. Elsevier B.V.: 608–16. doi:10.1016/j.seppur.2015.10.056.

Jarusutthirak, Chalor, Gary Amy, and Jean-Philippe Croué. 2002. "Fouling Characteristics of Wastewater Effluent Organic Matter (EfOM) Isolates on NF and UF Membranes." *Desalination* 145 (1–3): 247–55. doi:10.1016/S0011-9164(02)00419-8.

Jones, Kimberly L., and Charles R. O'Melia. 2000. "Protein and Humic Acid Adsorption onto Hydrophilic Membrane Surfaces: Effects of pH and Ionic Strength." *Journal of Membrane Science* 165 (1): 31–46. doi:10.1016/S0376-7388(99)00218-5.

Kang, Guo-dong, and Yi-ming Cao. 2012. "Development of Antifouling Reverse Osmosis Membranes for Water Treatment: A Review." *Water Research* 46 (3): 584–600. doi:10.1016/j.watres.2011.11.041.

Kao, C. M., B. M. Yang, R. Y. Surampalli, and Tian C. Zhang. 2012. "Limitation of Membrane Technology and Prevention of Membrane Fouling." In *Membrane Technology and Environmental Applications*, 504–32. Reston, VA: American Society of Civil Engineers.

doi:10.1061/9780784412275.ch17.

Lee, Young Ki, Young June Won, Jae Hyun Yoo, Kyung Hyun Ahn, and Chung Hak Lee. 2013. "Flow Analysis and Fouling on the Patterned Membrane Surface." *Journal of Membrane Science* 427. Elsevier: 320–25. doi:10.1016/j.memsci.2012.10.010.

Lim, A. L., and Renbi Bai. 2003. "Membrane Fouling and Cleaning in Microfiltration of Activated Sludge Wastewater." *Journal of Membrane Science* 216 (1–2): 279–90. doi:10.1016/S0376-7388(03)00083-8.

Maruf, Sajjad H., Melissa Rickman, Liang Wang, John Mersch IV, Alan R. Greenberg, John Pellegrino, and Yifu Ding. 2013. "Influence of Sub-Micron Surface Patterns on the Deposition of Model Proteins during Active Filtration." *Journal of Membrane Science* 444. Elsevier: 420–28. doi:10.1016/j.memsci.2013.05.060.

Maruf, Sajjad H., Liang Wang, Alan R. Greenberg, John Pellegrino, and Yifu Ding. 2013. "Use of Nanoimprinted Surface Patterns to Mitigate Colloidal Deposition on Ultrafiltration Membranes." *Journal of Membrane Science* 428. Elsevier: 598–607. doi:10.1016/j.memsci.2012.10.059.

Petronis, Šarūnas, Kent Berntsson, Julie Gold, and Paul Gatenholm. 2000. "Design and Microstructuring of PDMS Surfaces for Improved Marine Biofouling Resistance." *Journal of Biomaterials Science, Polymer Edition* 11 (10). Taylor & Francis Group : 1051–72. doi:10.1163/156856200743571.

Ro, Hyun Wook, Vera Popova, Lei Chen, Aaron M. Forster, Yifu Ding, Kyle J. Alvine, Dave J. Krug, Richard M. Laine, and Christopher L. Soles. 2011. "Cubic Silsesquioxanes as a Green, High-Performance Mold Material for Nanoimprint Lithography." *Advanced Materials* 23 (3). WILEY-VCH Verlag: 414–20. doi:10.1002/adma.201001761.

Sagle, Alyson C., Elizabeth M. Van Wagner, Hao Ju, Bryan D. McCloskey, Benny D. Freeman, and Mukul M. Sharma. 2009. "PEG-Coated Reverse Osmosis Membranes: Desalination Properties and Fouling Resistance." *Journal of Membrane Science* 340 (1–2): 92–108. doi:10.1016/j.memsci.2009.05.013.

Sayed, S K I. 2010. “OPTIMUM OPERATION CONDITIONS OF DIRECT CAPILLARY NANOFILTRATION FOR WASTEWATER TREATMENT” 14. http://www.iwtc.info/2010_pdf/08-04.pdf.

Šereš, Zita, Dragana Šoronja Simović, Ljubica Dokić, Lidietta Giorno, Biljana Pajin, Cecilia Hodur, and Nikola Maravić. 2016. “Edible Oil Industry Wastewater Treatment by Microfiltration with Ceramic Membrane.” *World Academy of Science, Engineering and Technology, International Journal of Chemical, Molecular, Nuclear, Materials and Metallurgical Engineering* 10 (4): 410–13. https://waset.org/Publication/edible-oil-industry-wastewater-treatment-by-microfiltration-with-ceramic-membrane/10004151.

Singh, Rajindar. 2006. *Hybrid Membrane Systems for Water Purification : Technology, Systems Design and Operation*. Elsevier.

Stroock, Abraham D., Stephan K. W. Dertinger, Armand Ajdari, Igor Mezić, Howard A. Stone, and George M. Whitesides. 2002. “Chaotic Mixer for Microchannels.” *Science* 295 (5555). http://science.sciencemag.org/content/295/5555/647.

Verliefde, Arne, Emile Cornelissen, Gary Amy, Bart Van Der Bruggen, and Hans Van Dijk. 2017. “Priority Organic Micropollutants in Water Sources in Flanders and the Netherlands and Assessment of Removal Possibilities with Nanofiltration.” Accessed April 21. doi:10.1016/j.envpol.2006.01.051.

Vogelaar, L., J.N. Barsema, C.J.M. van Rijn, W. Nijdam, and M. Wessling. 2003. “Phase Separation Micromolding—PSμM.” *Advanced Materials* 15 (16). WILEY-VCH Verlag: 1385–89. doi:10.1002/adma.200304949.

Vogelaar, Laura, Rob G. H. Lammertink, Jonathan N. Barsema, Wietze Nijdam, Lydia A. M. Bolhuis-Versteeg, Cees J. M. van Rijn, and Matthias Wessling. 2005. “Phase Separation Micromolding: A New Generic Approach for Microstructuring Various Materials.” *Small* 1 (6). WILEY-VCH Verlag: 645–55. doi:10.1002/smll.200400128.

Vrijenhoek, Eric M, Seungkwan Hong, and Menachem Elimelech. 2001. “Influence of Membrane Surface Properties on Initial Rate of Colloidal Fouling of Reverse Osmosis and Nanofiltration

Membranes." *Journal of Membrane Science* 188: 115–28. http://citeseerx.ist.psu.edu/viewdoc/download?doi=10.1.1.515.5946&rep=rep1&type=pdf.

Vrouwenvelder, J.S., J.A.M. van Paassen, L.P. Wessels, A.F. van Dam, and S.M. Bakker. 2006. "The Membrane Fouling Simulator: A Practical Tool for Fouling Prediction and Control." *Journal of Membrane Science* 281 (1): 316–24. doi:10.1016/j.memsci.2006.03.046.

Wang, Zhen, and Yifu Ding. 2010. "Probing Polymer Deformation Profiles at Varying Depths in Nanoimprint Lithography." *Nanotechnology* 21 (10). IOP Publishing: 105301. doi:10.1088/0957-4484/21/10/105301.

Weinman, Steven T., and Scott M. Husson. 2016. "Influence of Chemical Coating Combined with Nanopatterning on Alginate Fouling during Nanofiltration." *Journal of Membrane Science* 513: 146–54. doi:10.1016/j.memsci.2016.04.025.

Won, Young June, Seon Yeop Jung, June Hee Jang, Jae Woo Lee, Hee Ro Chae, Dong Chan Choi, Kyung Hyun Ahn, Chung Hak Lee, and Pyung Kyu Park. 2016. "Correlation of Membrane Fouling with Topography of Patterned Membranes for Water Treatment." *Journal of Membrane Science* 498: 14–19. doi:10.1016/j.memsci.2015.09.058.

Won, Young June, Jaewoo Lee, Dong Chan Choi, Hee Ro Chae, Inae Kim, Chung Hak Lee, and In Chul Kim. 2012. "Preparation and Application of Patterned Membranes for Wastewater Treatment." *Environmental Science and Technology* 46 (20): 11021–27. doi:10.1021/es3020309.

Xie, Peng, Lawrence Murdoch, and David Ladner. 2016. "Comparison of Computational Fluid Dynamics (CFD) and Experimental Data for Fouling Mitigation with Sinusoidal Reverse Osmosis Spacer." *(In Process)*. Accessed November 2. http://www.awwa.org/portals/0/files/education/conferences/membrane/mtc16/membrane papers/wed09 papers/03-xie paper.pdf.

Xu, Pei, Jörg E. Drewes, Tae-Uk Kim, Christopher Bellona, and Gary Amy. 2006a. "Effect of Membrane Fouling on Transport of Organic Contaminants in NF/RO Membrane Applications." *Journal of Membrane Science* 279 (1): 165–75.

doi:10.1016/j.memsci.2005.12.001.

———. 2006b. “Effect of Membrane Fouling on Transport of Organic Contaminants in NF/RO Membrane Applications.” *Journal of Membrane Science* 279 (1): 165–75. doi:10.1016/j.memsci.2005.12.001.

Yongki Shim, Hong-Joo Lee, Sangyoup Lee, and Seung-Hyeon Moon, and Jaeweon Cho*. 2002. “Effects of Natural Organic Matter and Ionic Species on Membrane Surface Charge.” American Chemical Society . doi:10.1021/ES015880B.

Zhang, Yang, Luc Pinoy, Boudewijn Meesschaert, and Bart Van der Bruggen. 2013. “A Natural Driven Membrane Process for Brackish and Wastewater Treatment: Photovoltaic Powered ED and FO Hybrid System.” *Environmental Science & Technology* 47 (18): 130904084026001. doi:10.1021/es402534m.

DECLARATION OF ACADEMIC HONESTY

I, RASNA SHARMIN, hereby confirm that the document in hand titled "DEVELOPMENT OF COMPUTATIONAL FLUID DYNAMICS (CFD) MODELS FOR SIMULATING FOULANT REDUCTION BY PATTERNED RO AND NF MEMBRANES" is solely my own work and that every text passage, figure or diagram from books, papers, the Web or any other source copied or in any other way used has been acknowledged and fully cited.

Rasna Sharmin (Date: 24.04.2017...)

SIGNATURE Rasna Sharmin 24/04/2017